ACID FRACTURING CARBONATE-RICH SHALE: A FEASIBILITY INVESTIGATION OF EAGLE FORD FORMATION

A Thesis

by

RACHAEL JEANENE CASH

Submitted to the Office of Graduate and Professional Studies of
Texas A&M University
in partial fulfillment of the requirements for the degree of

MASTER OF SCIENCE

Chair of Committee,	Ding Zhu
Committee Members,	A. Daniel Hill
	Yuefeng Sun
Head of Department,	A. Daniel Hill

August 2016

Major Subject: Petroleum Engineering

ABSTRACT

Due to the extensive technically recoverable shale natural gas resources and an increase in production from shale plays over the last 10 years, it is essential to focus on stimulation techniques to enhance productivity in shale resources. One such stimulation technique is acid fracturing. Similar to hydraulic fracturing, acid fracturing injects acid into a formation at a pressure greater than the fracture pressure, creating fractures and etching the created fracture face. The high carbonate content of the Eagle Ford Shale makes the formation a possible acid fracturing candidate. Minimal research has been completed on the effects of acid fracturing high carbonate-containing shale formations, where various conditions can limit the permeability of petroleum fluids. In this study, eight Eagle Ford shale samples, four from Zone C and four from Zone D, are used to determine the effect of surface etching pattern, acid concentration, calcite content, and Brinell Hardness Number on created acid fracture conductivity in the Eagle Ford shale.

The resultant surface etching volume is determined by a pre-and post-surface Profilometer scan to calculate the change in surface profile. Calcite content is determined by X-Ray Diffraction analyses. Conductivity tests are performed on the eight samples up to a closure stress of 4000 psi, sample integrity permitting.

Based on the results determined in this study, acid fracturing the Eagle Ford shale could provide optimistic increases in production. Acid fracturing treatments in high calcite containing zones of the Eagle Ford shale are expected to result in an increase in productivity. For the Eagle Ford Shale, the surface etching patterns that result in

highly sustained conductivity values are channeling and roughness. A direct correlation is shown between calcite content of the shale and resultant surface etching volume. Furthermore, the higher the calcite content of the samples, the more likely the etching pattern will result in channeling and surface roughness. Brinell Hardness tests are completed on Eagle Ford samples determining that, on average, the higher the Brinell Hardness number, the better resulting surface etching pattern and sustained acid fracture conductivity.

DEDICATION

To God, without whom none of this would be possible. To my parents and sister for their continual support. And to Dr. G.T. Lineberry for teaching me to pursue my dreams.

ACKNOWLEDGMENTS

I would like to express my thankfulness to Dr. Ding Zhu and Dr. A. Daniel Hill for granting me the opportunity to participate in this research and for their continual support throughout my graduate school career. Thanks also to Dr. Sun for serving on my committee.

Thanks to the Acid Fracturing group: Xichen Wang, Assiya Suleminova, and Ingrid Hornickle.

Thanks to the Hydraulic Fracturing group for providing the Eagle Ford outcrop samples and Ashley Knorr for help with Brinell Hardness tests.

NOMENCLATURE

Acronyms

BHN	Brinell Hardness Number
CO_2	Carbon Dioxide
DREC	Dissolved Rock Equivalent Conductivity
°F	Fahrenheit
FTIR	Fourier Transformed Infrared Spectroscopy
HCl	Hydrochloric Acid
MICP	Mercury Injection Capillary Pressure
RES	Rock Embedment Strength
SRV	Stimulated Reservoir Volume
XRD	X-Ray Diffraction

Variables

h	Height of fracture, in
k_{fw}	Fracture conductivity, md-ft
L	Length of fracture, in
M	Molecular mass, kg/kg-mol
q	Flow rate, liter/s
R	Universal constant
T	Temperature, °K
w	Fracture width, in
v	Fracture flow velocity, ft/s
Z	Compressibility factor

μ	Viscosity, cP or Pa-s
ϱ	Density, lb/ft^3 or kg/m^3

TABLE OF CONTENTS

Page

ABSTRACT……...……..…….….ii

DEDICATION……..……....iv

ACKNOWLEDGMENTS..…….…...v

NOMENCLATURE..……...…....vi

TABLE OF CONTENTS..…….…viii

LIST OF FIGURES..…….....x

LIST OF TABLES...……...……xiii

CHAPTER I INTRODUCTION AND LITERATURE REVIEW 1

1.1 Acid Fracturing and Created Conductivity 1
1.2 Literature Review 6
1.3 Problem Description 17
1.4 Objectives of Research 17

CHAPTER II EXPERIMENTAL SETUP, PROCEDURES AND CONDITIONS 19

2.1 Experimental Set Up 19
2.2 Experimental Procedure 24
2.3 Core Sample Preparation 25
2.4 Surface Characterization 27
2.5 Acid Etching 27
2.6 Acid Fracture Conductivity Measurement and Calculation 32
2.7 Experimental Conditions 37

CHAPTER III EXPERIMENTAL RESULTS AND DISCUSSION 40

3.1 Case Study Background 40
3.2 Sample Description 43
3.3 Results for Test Conditions #1 and #2 44
3.3.1 EF_C_1 44
3.3.2 EF_C_2 47
3.3.3 EF_C_3 49
3.3.4 Comparison of Zone C Results 51
3.3.5 EF_D_1 52
3.3.6 EF_D_2 55
3.3.7 EF_D_3 57
3.3.8 Comparison of Zone D Results 59
3.4 Results for Test Condition #3 60
3.4.1 EF_C_4 60
3.4.2 EF_D_4 62
3.5 Parametric Study of Acid Fracturing Conductivity in the Eagle Ford Shale 65
3.5.1 Effect of Etching Pattern on Acid Fracture Conductivity 65
3.5.2 Effect of Acid Concentration on Acid Fracture Conductivity 69
3.5.3 Effect of Calcite Content on Acid Etching and Acid Fracture Conductivity 71
3.5.4 Effect of Rock Strength Properties on Acid Fracture Conductivity 74
3.5.5 Comparison with Tripathi and Pournik Study 77

CHAPTER IV CONCLUSION AND FUTURE WORK 81

4.1 Conclusion and Future Work 81

REFERENCES 83

APPENDIX A 89

i. Eagle Ford X-Ray Diffraction Results: Zone D Sample 1 89
ii. Eagle Ford X-Ray Diffraction Results: Zone D Sample 2 90
iii. Eagle Ford X-Ray Diffraction Results: Zone C Sample 1 91
iv. Eagle Ford X-Ray Diffraction Results: Zone C Sample 2 92

LIST OF FIGURES

Page

Fig. 1: Acid Fracture Process..... 1

Fig. 2: Dependence of Resulting Conductivity. 2

Fig. 3: Packing Structures of Calcite and Dolomite. 4

Fig. 4: Fracture Stress Distribution. 10

Fig. 5: Fourier transform Infrared Spectroscopy Analysis Results. 13

Fig. 6: Created Fracture Surface. 19

Fig. 7: Test Cell and Core Samples used in this Study. 20

Fig. 8: Acid Fracturing Lab Setup 21

Fig. 9: Acid Fracturing Apparatus. 22

Fig. 10: Conductivity Laboratory Setup. 23

Fig. 11: Acid Fracturing Experimental Process 25

Fig 12: Profilometer Setup. 27

Fig 13: Chem/Meter 800 Series Pump 30

Fig 14: Zones of the Eagle Ford Shale with Corresponding Gamma Ray Response at the Lozier Canyon BP Field Site..... 41

Fig. 15: Location of Sample Obtainment (left) and Description of Zones C and D of the Eagle Ford Shale. 42

Fig. 16: Post Sample Surface Image and Difference in Surface Profile of EF_C_1. 45

Fig. 17: Acid Fracture Conductivity for EF_C_1 46

Fig. 18: Post Sample Surface Image and Difference in Surface Profile of EF_C_2. 47

Fig. 19: Acid Fracture Conductivity for EF_C_2 49

Fig. 20: Post Sample Surface Image and Difference in Surface Profile of EF_C_3. 50

Fig. 21: Acid Fracture Conductivity for EF_C_3 51

Fig. 22: Acid Fracture Conductivity for EF_C_3 52

Fig. 23: Post Sample Surface Image and Difference in Surface Profile of EF_D_1. 53

Fig. 24: Acid Fracture Conductivity for EF_D_1 54

Fig. 25: Post Sample Surface Image and Difference in Surface Profile of EF_D_2. 55

Fig. 26: Acid Fracture Conductivity for EF_D_2 56

Fig. 27: Post Sample Surface Image and Difference in Surface Profile of EF_D_3. 57

Fig. 28: Acid Fracture Conductivity for EF_D_3 58

Fig. 29: Acid Fracture Conductivity for Zone D (EF_D_3 Contains Error) 59

Fig. 30: Post Sample Surface Image and Difference in Surface Profile of EF_C_4. 61

Fig. 31: Acid Fracture Conductivity for EF_C_4 62

Fig. 32: Post Sample Surface Image and Difference in Surface Profile of EF_D_4. 63

Fig. 33: Acid Fracture Conductivity for EF_D_4 64

Fig. 34: Four Observed Etching Patterns 65

Fig. 35: Effect of Surface Etching Amount on Sustained Acid Fracture Conductivity 66

Fig. 36: Effect of Surface Structure on Conductivity..... 67

Fig. 37: Effect of Surface Structure on Conductivity..... 68

Fig. 38: Eagle Ford Test Results for Test Conditions #1 and #2 (EF_D_1 is not shown) 71

Fig. 39: X-Ray Diffraction Analysis Results for Eagle Ford Shale Zones C and D 72

Fig. 40: Effect of Calcite Content on Surface Etching Volume 73

Fig. 41: Effect of Calcite Content on Sustained Conductivity 73

Fig. 42: X-Ray Diffraction of Zones C and D Comparison of Smaller Mineral Composition Contributions..... 74

Fig. 43: Hardness Results for Eagle Ford Shale Samples..... 75

Fig. 44: Hardness and Resulting Sustained Conductivity for Eagle Ford Shale Samples..... 76

Fig. 45: Comparison of Acid Fracture Conductivity Results with Tripathi and Pournik Study (2014) 79

LIST OF TABLES

Page

Table 1: Variables Used for Conductivity Calculations 37

Table 2: Experimental Test Conditions 38

Table 3: Test Conditions Used for each Sample 38

Table 4: Description of Eagle Ford Samples from Current Study 43

Table 5: Total Left and Right Etching Volumes (in^3) 44

Table 6: Total Left and Right Etching Volumes (in^3) 60

Table 7: Resulting Conductivity for Varying Acid Concentrations in Test Condition #1 and #2 69

Table 8: Comparison of Experimental Conditions 78

Table 9: Etching and Conductivity Results for Test Condition #3 79

CHAPTER I

INTRODUCTION AND LITERATURE REVIEW

1.1 Acid Fracturing and Created Conductivity

An estimated 610 Tcf of technically recoverable shale natural gas resources and 59 billion barrels of technically recoverable tight oil resources are available from U.S. shale plays (EIA, 2014). To produce this unconventional resource, well stimulation is necessary. Acid fracturing has proved effective in increasing the conductivity of carbonate reservoirs due to the composition of carbonate formations and its reactivity with acid. Similar to hydraulic fracturing, acid fracturing injects acid into a formation at a pressure greater than the fracture pressure, creating fractures and etching the created fracture faces. The methodology of acid fracturing is shown in **Fig. 1**.

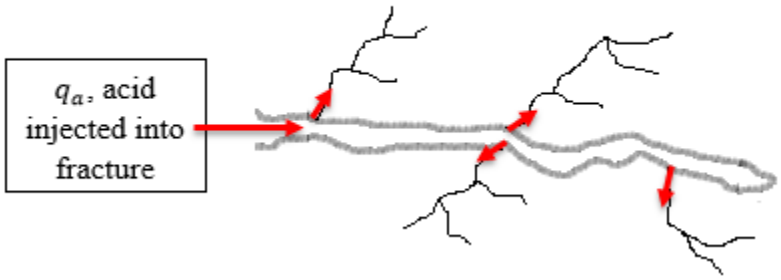

Fig. 1: Acid Fracture Process

In Fig. 1, the injected acid moves through the fractures, reacting with the exposed surface area of the fracture and propagating further into the fracture. As the acid is introduced to the fracture faces, the acid initially reacts with the surface of the exposed

rock but also reacts further into the rock as the acid front continues dissolving the rock in a process called differential etching. After the fracture pumping is finished, the fracture is able to remain open, supported by the uneven surface that is created by differential etching. (Economides et al., 2012).

Unlike hydraulic fracturing, acid fracturing does not rely on proppant to maintain open fractures. Acid fracture conductivity relies on roughness of the fracture surface after etching, which is related to formation rock heterogeneity (permeability and mineralogy distribution) and leak-off during acid fracturing, shown in **Fig. 2**.

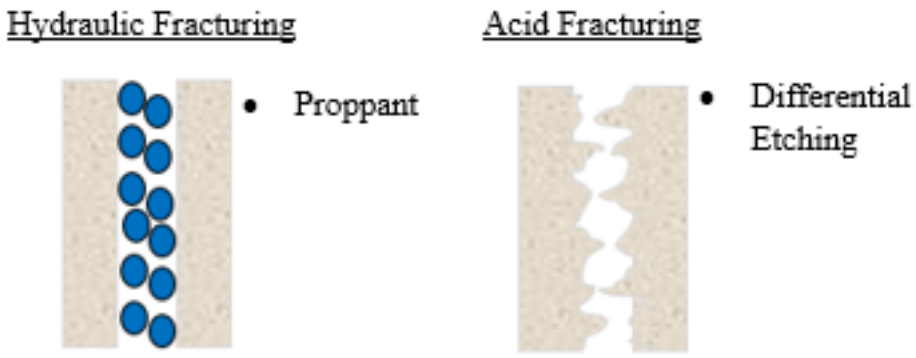

Fig. 2: Dependence of Resulting Conductivity. Modified from Deng et al., 2011.

Acid fracturing shale plays has the ability to better reach the natural fractures existing within the formation that are unreachable in hydraulic fracturing. By reaching microfractures in acid fracturing, the stimulated reservoir volume (SRV) is increased, therefore increasing the productivity.

The Eagle Ford shale is a carbonate-rich formation. Calcite content in the producing zone, B, averages 70% (Gehring, 2016) determined by X-Ray Diffraction (XRD). For the zone C and D samples used in this study, the calcite content averaged 75% and 83%, respectively, also determined by X-Ray Diffraction analysis.

Through acid fracturing shale formations, the carbonate material in the shale will be dissolved, acting in a similar manner to carbonate acid fracturing. HCl is the most widely used acid type in acid fracturing due to its availability and low cost. The chemical reactions of calcite ($CaCO_3$) and dolomite ($CaMg(CO_3)_2$) with HCl are shown in **Eq. 1 and Eq. 2**, respectively.

$$2HCl_{(aq)} + CaCO_{3_{(s)}} \xrightarrow{yields} CaCl_{2_{(s)}} + CO_{2_{(g)}} + H_2O_{(l)} \quad \text{(eq. 1)}$$

$$4HCl_{(aq)} + CaMg(CO_3)_{2_{(s)}} \xrightarrow{yields} CaCl_{2_{(s)}} + MgCl_{2_{(s)}} + CO_{2_{(g)}} + H_2O_{(l)} \quad \text{(eq. 2)}$$

Though both minerals have a high reaction rate when exposed to acid, the HCl-calcite reaction occurs more quickly than the HCl-dolomite reaction. The HCl-calcite reaction is mass-transfer limited, as the reaction is controlled by the transportation of the acid to the rock face. The reaction rate of HCl-dolomite is surface-transfer limited, as the reaction rate of the acid on the exposed rock face is the limiting reaction. The reaction between dolomite-HCl is also more sensitive to temperature than the HCl-calcite reaction (Newman et al., 2009). These differences in reaction are due to the tighter packing structure of dolomite as compared to calcite (Gomaa and Nasr-El-Din, 2009) and the stronger bond between oxygen and magnesium in dolomite due to higher Van

der Waals forces. Van der Waals forces act as attractive forces, creating a stronger bond between the oxygen and magnesium molecules. The packing structures of calcite and dolomite are shown in **Fig. 3**.

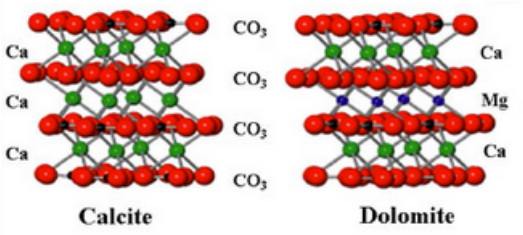

Fig. 3: Packing Structures of Calcite and Dolomite. Magalhaes et al., 2013.

Due to the high calcite content in the Eagle Ford shale, it is concluded that the reaction between HCl and high calcite containing shale formations is mass-transfer limited and best results can be achieved using the highest possible injection rate. At the highest possible injection rate, the acid travels by convection which requires a smaller volume of acid needed.

Prior to acid fracturing shale formations, it is important to determine the carbonate content of the rock. Without sufficient carbonate in the shale, the acid fracturing results will be futile. Careful considerations for acid concentration, test duration, and formation temperature should be made. Depending upon the carbonate content of the shale, the reaction between the rock and acid could create inefficient channels that are not able to provide sufficient conductivity. For calcite-rich shale like the Eagle Ford, both microfractures and hydraulic fractures are stimulated by acid

without the use of proppant. The varying mineralogy of the Eagle Ford shale allows for surface dissolution from the HCl-calcite interaction. By dissolving the calcite, inactive minerals such as quartz and clay remain and act as pillars to prop the fracture open under closure stress.

The characteristics of the acid fracture created are dependent upon multiple conditions including: acid selection, injection rate, leak-off rate, and in-situ formation conditions such as rock stress distribution. The success of acid fracturing is dependent upon the surface etching volume, surface etching pattern, and the ability of fractures to remain open over time. Sustaining fracture conductivity over time is directly related to initial acid selection considerations for creating efficient width acid fractures. Generally, the wider the created fracture, the more likely it is to remain open over time. This is due to stability support that results from the undissolved rock. With the creation of narrow fractures, sustaining fracture conductivity over time is less likely. Furthermore, if the well is in a high-stress area, such as is the case for a deep well, the fractures could eventually close. Acid fracturing treatment success is also dependent upon the rock mechanics properties of the rock. Typically exhibiting a lower Brinell Hardness Number than purely carbonate formations, shale is fissile and can break easily. Using higher concentrations of HCl in the shale samples can cause a decrease in rock strength properties which causes fracture collapse under higher closure stress.

There has been minimal work completed on acid fracturing shale formations. Through a review of previous research in both acid fracturing carbonate and shale formations, suggestions for acid fracturing shale formations is given. An experimental

investigation of acid fracturing high-carbonate containing shale samples is determined in this study. The experimental results can be applied to field scale applications.

1.2 Literature Review

There have been studies on acid fracturing in shale formations. In a study by Wu and Sharma (2015), research was conducted to determine the effect of acid fracturing on carbonate-rich shale formations. The study addresses the following four problems:

-Does acid fracturing improve the productivity of microfractures in carbonate-rich shale?

-What kinds of structure or surface pattern can develop when carbonate minerals are dissolved?

-How would acid fracturing affect minerals like clay, quartz, and organic matter that are present in high abundance in a shale but do not react with acid?

-How would the pore structure change in acid fracturing?

For the Bakken shale samples used in the study, 24 wt. % of the rock matrix was composed of carbonate minerals. Microstructure, pore structure and petro physical properties were compared for a core divided into an acidized section and an un-acidized section. Emission scanning electron microscope (FE-SEM) was used to observe shale properties and pore structure before and after acid fracturing. FE-SEM provides topographical and compositional information at a resolution of down to 1 ½ nanometers (PhotoMetrics, Inc., 2016). Pore structure was further determined using mercury intrusion porosimetry (MIP) and nitrogen absorption with crushed samples. The sample size, experimental setup, and acid type and concentration used in the study varies

substantially from this study. Bakken cores were cut into 0.25-inch thick disks of 2.5-inch inner diameter to be used in an acidizing cell. In the acidizing cell, 3-wt%HCl in 3-wt%KCl was pumped at 20ml/min with a differential pressure of 100-120 psi to move acid through the sample. An indentation test was also conducted to determine the hardness of the pre- and post-acid treatment core sample. Acid was applied to individual faces of two 0.25-inch disks in durations of 1-hour and 24-hour long tests. Indentation tests were applied at five random places for each sample. The hardness of the sample was calculated by determining the maximum applied load divided by the total contact area of the maximum indentation made on the sample. Wu and Sharma found four different distributions of carbonates in the Bakken core samples. Those descriptions and the resulting surface after acid fracturing include:

(1) Carbonate-rich regions, with area over 100 micrometers x 100 micrometers containing mostly fine grained limestone muds, or associated with calcite precipitation in natural fractures

Result After Acidizing: channels, 30-50 micrometers deep with pits ranging from 1-8 micrometer

(2) Carbonate islands, with dimensions of around 10 to 30 micrometers

Result After Acidizing: cavities, 10-30 micrometers deep

(3) Carbonate rings, at the rim of quartz or clay grains or clusters of grains with dimensions of 10 to 30 micrometers

Result After Acidizing: grooves, some dislodged inert minerals

(4) Finely mixed siliceous and carbonate grains

Result After Acidizing: rough surface, could possibly create a well-connected flow network

The surface of sections containing carbonates and inert minerals resulted in a small etching surface roughness; however, little to no changes were noted with the inert minerals alone.

Wu and Sharma found that pore size increases in carbonate rocks in shale formations after acid fracturing. Acidizing resulted in the enlargement of pore size, with the largest resulting pores being macropores up to 120 micrometers. In the matrix, macropores were enlarged, giving access to mesopores and leading to an expected increase in permeability and porosity. No pore structure changes resulted in clay, quartz, or organic matter. Acidizing did help to reach the inert pores that were under carbonate cement, as in the case of the rough surface created in finely mixed siliceous and carbonate grains. In the acidized section of the core tested using Mercury Intrusion Porosimetry and nitrogen absorption, approximately 76.6% of the dissolved solids were carbonates, the other were inert minerals. From the indentation tests, it was determined that exposure to acid for 1-hour and 24-hours can reduce hardness to 71% and 37% of the original value, respectively. Considering rock mechanics properties, the application of acid did not result in changes to Young's Modulus. Critical factors on the success of acid fracturing shale are dependent on mineralogy and pore structure of the carbonate-rich shale and how those factors change throughout the fracturing process. The replicability of this study would be difficult because the success of the increase in pore

size is completely dependent upon the carbonate content in the shale formation. Due to the heterogeneity of shale, an additional study could have substantially different results.

Success of acid fracturing depends how well the fracture can remain open under closure stress, which is directly correlated with the degree of surface asperities created on the fracture face. When acid fracturing creates an etched face, Abass et al. (2006) suggested that obtaining a successful conductive fracture is dependent on the overall reaction of the carbonate formation and acid (or in the case of this study, the carbonate in shale formations), the surface etching pattern, reaction to horizontal stress, and how the rock formation behaves elastically. The way the rock face is etched has a major influence on how the rock will behave under closure stress, (Antelo et al., 2009). Before concluding an increase in productivity, it is essential to test the acid fractured shale cores in a conductivity test while considering rock mechanics properties.

In the study by Abass et al. (2006), the rock mechanics effects of formations under closure stress after acid fracturing carbonate formations were studied. Since there is a lack of research in the field of acid fracturing shale formations, this is a suitable comparison as the predominant dissolved rock in acid fracturing shale is carbonate. Fracture closure is due to failure and crushing of the asperities, or undissolved contact points of the rock face in the fracture, under horizontal stress and creep. Abass et al. (2006) tested different core samples in the lab by recreating in-situ conditions. The effects of acid on the rock mechanics properties of rock was determined by considering the effect of acid fracturing through three stages of deformation: elastic, plastic, and

creep. As shown in **Fig. 4,** under closure stress the created fracture is exposed to additional stress, as the stress field is stronger around the created fracture.

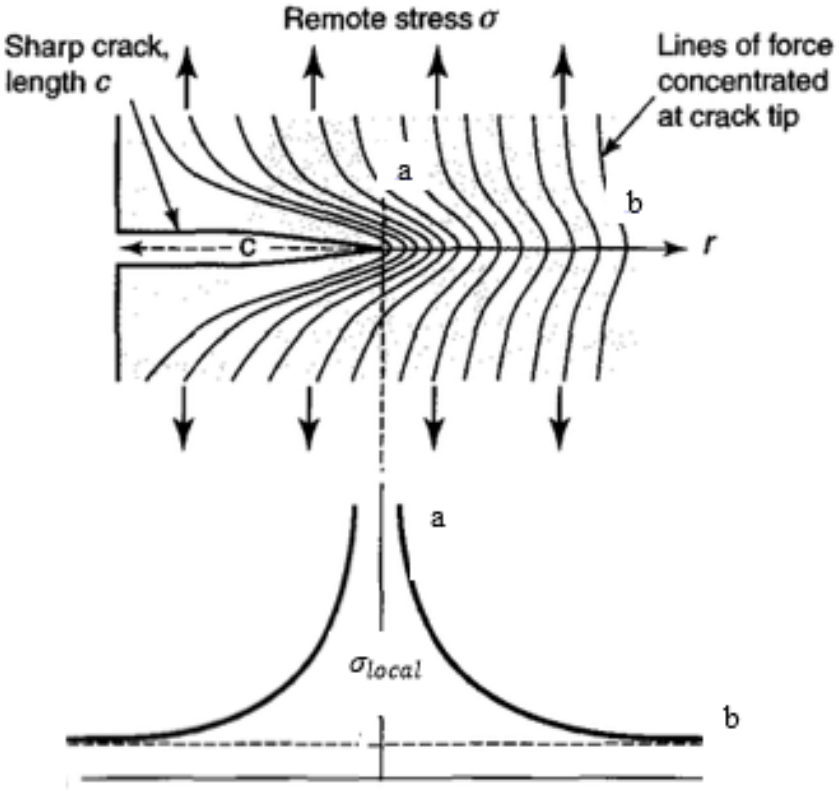

Fig. 4: Fracture Stress Distribution. From Ashby et al., 2013

The local stress increases along the fracture, and decreases outward away from the fracture, toward intact rock. As the closure stress increases around the fracture, the rock exposed to acid will behave either elastically or plastically. If the rock behaves elastically, it will be able to support the additional horizontal stress, failing to surpass its yield strength. If the rock sustains plastic deformation, the rock will become brittle, unable to sustain the additional horizontal stress, reaching the failure point. As the strain in the rock increases, the rock will be more likely to exhibit plastic deformation. The

fracture will also be subjected to creep, the response of the fracture to horizontal stress exposure over time. As application of constant closure stress is continued, creep can cause the fracture to displace, building up additional stress in the asperities, resulting in failure or crushing of the asperities. Creep was tested by applying consecutive horizontal stress values to the rock to determine the overall rock displacement. Using the Burgers model (Goodman, 1980) to determine strain over time under a constant stress, Abass et al. found that nonlinear behavior for creep resulted. They suggested using the Brinell Hardness Number to determine if acid fracturing is an efficient choice. Brinell Hardness Number helps to determine the strength properties of the rock. When acid weakens the strength of a low Brinell Hardness Number rock, the asperities are also weakened, which can lead to failure in sustaining the fracture conductivity. Creep is common in rocks with lower Young's modulus where acid can weaken the fracture face to the point that the addition of closure stress can lead to failure between surface asperities. The rock begins to behave plastically instead of elastically and can reach failure. The crushing of the rock can also lead to fines that block pores and decrease permeability.

The deformation and creep behavior of carbonate-rich shale plays vary because rock strength properties are heterogeneous. The varying result of surface etching patterns will lead to differences in sustaining fracture conductivity over time. Contact ratios of asperities would be higher for carbonate-rich regions, as defined by Wu and Sharma (2015), (1) and carbonate islands (2), where channels and cavities were formed, respectively. However, in carbonate formations, a larger volume of dissolved rock does not always yield higher conductivity (Abass et al., 2006), as is the case for the deeper

channels in limestone. When closure stress is applied to the rock, the rock can fail as stress builds up in the asperities. Therefore, a likely assumption for carbonate-rich shale formations would be that the (1) and (2) regions from the study would fail under lower closure stress as compared to the (3) and (4) regions. Additionally, stronger rock with higher Brinell Hardness Number, such as Quartz in region (3) would be expected to remain open under higher closure stress.

Tripathi and Pournik (2014) also studied the effects of acid fracturing the Eagle Ford Shale formation injecting 15 wt.% HCl into fractures of different widths, with and without proppant, on four 1.5 in. x 6 in. rough surface core samples. Due to the increase in closure stress due to production, Tripathi and Pournik observed that the secondary fractures within the Eagle Ford shale were unable to remain opened due to the lack of proppant placement. This lack of connectivity leads to limited production from the primary fractures only, as the smaller fractures are unable to feed into the larger fractures. 16 noted minerals found in the samples from Fourier transform infrared spectroscopy (FTIR) are shown in **Fig. 5**.

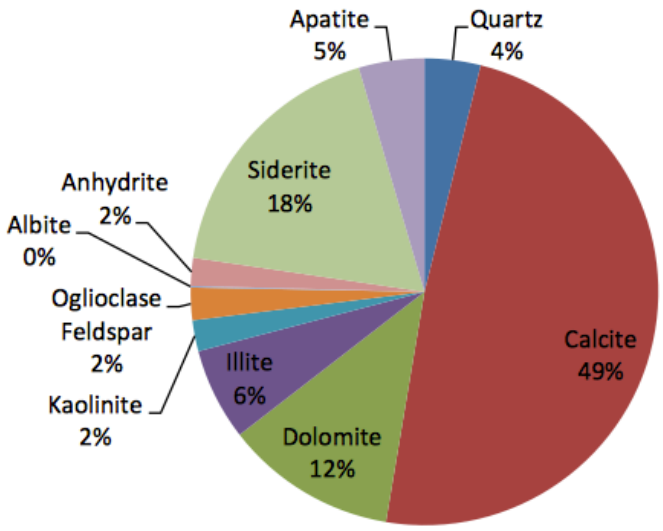

Fig. 5: Fourier transform infrared spectroscopy Analysis Results. From Tripathi and Pournik, 2014.

61 wt. % (49 wt. % calcite and 12 wt. % dolomite) of the sample mineralogy was soluble in 15 wt. % HCl. To determine pre-and post-acid pore characteristics, the samples were soaked in 15wt.% HCl for 24 hours at ambient temperatures and then characterized using Mercury Injection Capillary Pressure.

The initial methodology for acid fracturing the Eagle Ford shale is based upon acid fracturing carbonate formations due to the high calcite content in the formation. There has been substantial research focused on creating successful acid fracturing treatments in carbonates. Just as in carbonate formations, the conductivity of shale is highly dependent upon the resulting surface etching pattern after acid fracturing. In the work of Ruffet et al., (1998), fracture conductivity was estimated based on observing the amount of etching on the surface after acid exposure. In their study, varying concentrations of straight HCl, 5wt%, 7wt%, and 15wt. %, and 15wt. % gelled HCl were

used on Lavoux limestone and Brabant dolomite. The 5wt. % HCl sample had more non-uniform etching, while the gelled 15wt. % HCl sample had more uniform etching. Due to the more uniform etching pattern, the latter sample closed more quickly under closure stress. This study suggested that the more uniform etching, the lower resulting conductivity. Ruffet et al. suggested that the created roughness should be considered in fracture conductivity considerations as it effects how those fractures remain open over time.

Similar to Ruffet et al., Pournik et al. (2009) also considered the effect of the etching pattern occurring on the surface profile to conductivity in different rocks, including: Indiana limestone, Macae limestone, Bryozoan limestone, Texas Cream chalk, and San Andres dolomite. Different acid types were also used including: HCl, gelled acid, emulsified acid, and viscoelastic acid. Contact time between the acid and formation varied between 5 to 60 minutes. Contact ratios, the ratio of surface area of asperities that touch each other compared to the total fracture surface area, were determined for each sample. The study found that the higher the contact ratio, or more non-uniform etching, the higher the conductivity value. Rocks exhibiting a lower uniaxial compressive strength, such as limestone and chalk, had deeper etchings and wider fractures compared to dolomite, thus higher recorded contact ratios.

Using surface Profilometer scans, Antelo et al. (2009) determined sample surface roughness pre- and post-acid fracturing. They determined the geometry of the created etchings, instead of assuming average fracture width is the value of dissolved rock at zero closure stress. The study found that higher conductivity results from surface

channeling, or non-uniform etching, in the rock surface compared to samples sans channel formation. In the latter, the conductivity is more dependent upon the asperities of the rock. Due to the uniform nature of the surface etching, fewer asperities exist, making it more difficult for the created fracture to remain open under closure stress. Considering rock strength properties, Antelo et al. found that stronger rocks such as dolomite and high uniaxial compressive strength limestone have low fracture widths but can still have sufficient conductivity.

Rock mechanics properties of a sample are also influential factors on the resulting conductivity of the sample. The work of Gomaa and Nasr-El-Din (2009) derives correlations for determining fracture conductivity over time through considerations of rock mechanics properties of the rock. The study compares the Nierode and Kruk (1973) correlation with the Nasr-El-Din et al. (2008) correlation that has separate considerations for limestone and dolomite. Gomaa and Nasr-El-Din found that longer acid contact time for a rock does not necessarily yield higher conductivity. As the length of acid exposure is increased, the rock can weaken along the exposure face. Then as closure stress is applied, the weak rock can't support the fractures and closes, decreasing conductivity. The ability of the created fractures to remain open depends upon the rock mechanics properties of the rocks. The dissolved rock equivalent conductivity determines maximum conductivity and the rock embedment strength determines fracture conductivity under closure stress. The study found that limestone conductivity is more dependent upon rock embedment strength while dolomite conductivity is more dependent upon dissolved rock equivalent conductivity. Rock

embedment strength is the major determinate of the rock's response to closure stress; the higher the rock embedment strength, the lower response to closure stress. Limestone is a weaker rock than dolomite, therefore the rock embedment strength more important to limestone conductivity calculations. At a closure stress of zero, the conductivity of the rock is its dissolved rock equivalent conductivity value.

Although the majority of studies suggest that acid does weaken the rock face, Joel et al. (2011), suggests that there is no conclusive effect on if the acid weakens the rock face since the decrease values in rock embedment strength all fall within the suggested range of error. Through reviewing previous fracture conductivity correlations, Joel et al. determined that understanding the rock strength properties of the rocks is essential to determining how the fracture will remain open under stress. The strength properties measured for use in the correlations can vary and thus yield very different results. Rock embedment strength is the only rock strength property that has been widely used in correlations. It measures the resistance of a rock to plastic deformation by pushing a steel ball bearing into the surface of the rock at a length of the radius of the ball divided by the area of the bearing. Rock embedment strength values can vary greatly between correlations, formations, and even in individual formations due to the heterogeneity of rock. Joel et al. compared rock embedment strengths determined from the Nierode and Kruk (1973) and Nasr-El-Din et al. (2008) correlations. For Indiana limestone, the Nierode and Kruk correlation had a 13% error in rock embedment strength and the Nasr-El-Din et al. correlation had a 12% error. For San Andres dolomite, the Nierode and Kruk correlation had a 15% error in rock embedment strength

and the Nasr-El-Din et al. correlation had a 34% error. Joel et al. also determined that from the errors in rock embedment strength, the correlation values determined can be in error from 5% to 180%, depending on the correlation used, rock type, and closure stress applied. In order to better understand sustaining fracture conductivity in acid fractures, Joel et al. determined that more work should be done to understand acid effects on rock strength and a better way to quantify rock strength in correlations.

1.3 Problem Description

With the past success of acid fracturing treatments in carbonate formations, high carbonate-containing shale formations have the propensity to be successful acid fracturing candidates.

1.4 Objectives of Research

The objective of this research is to determine if there is a potential productivity increase from acid fracturing treatments in the Eagle Ford shale, a high carbonate containing formation. This will be determined through a lab scale test of acid fracturing treatments using different test conditions. Eight Eagle Ford shale samples, four from Zone C and four from Zone D, of 7” x 3” x 1.7” dimension will be used.

There are two main objectives of this study:

- Determine the effect of etching pattern, acid concentration, carbonate content, and Brinell Hardness number on the created acid fracture conductivity

- Determine potential feasibility of field-scale acid fracturing treatments in the Eagle Ford Shale

Using the data collected in this study, a comparison to the study of Tripathi and Pournik, 2014, will also be completed using the data from test condition #3. The experimental procedure by Wu and Sharma, 2015, varies too greatly to compare to the data collected in this study.

CHAPTER II

EXPERIMENTAL SETUP, PROCEDURES AND CONDITIONS

2.1 Experimental Set Up

The goal of this experimental study is to simulate an acid fracturing treatment in order to determine the effect of etching pattern, acid concentration, carbonate content, and Brinell Hardness Number on the created acid fracture conductivity.

Eagle Ford outcrops were obtained and cut to modified API-RP-61 conductivity cell specifications. Fracture simulation is achieved by the application of stress to the sample, where the fracture pressure is initiated. This process results in an initial rough surface on the left and right halves of the sample, as shown in **Fig 6**.

Fig. 6: Created Fracture Surface.

After the samples have been cut, a silicone-potting compound is applied to the outer surfaces of the sample to help protect sample integrity. The two fractured sample halves are placed in a modified API-RP-61 conductivity cell made of Hastelloy material.

The modified API-RP-61 conductivity cell is designed to hold 7-in. long, 1.7-in. high, and 3-in. thick samples. Due to the various strengths of acid used in the test, the cell is corrosion resistant to withstand acid application. The test cell and an example sample are shown in **Fig. 7.** To decrease acid leak-off in the acid fracturing test and nitrogen leaks in the conductivity test, two O-rings are used to ensure a tight fit for the samples. A description of the acid fracturing lab setup is shown in **Fig. 8**.

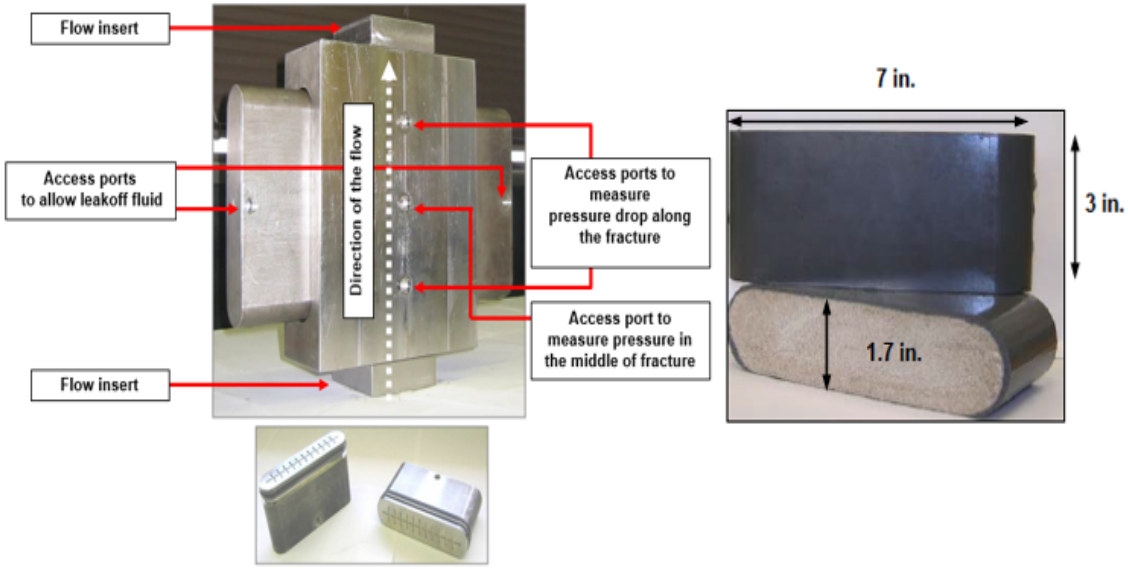

Fig. 7: Test cell and core samples used in this study. Melendez, 2007.

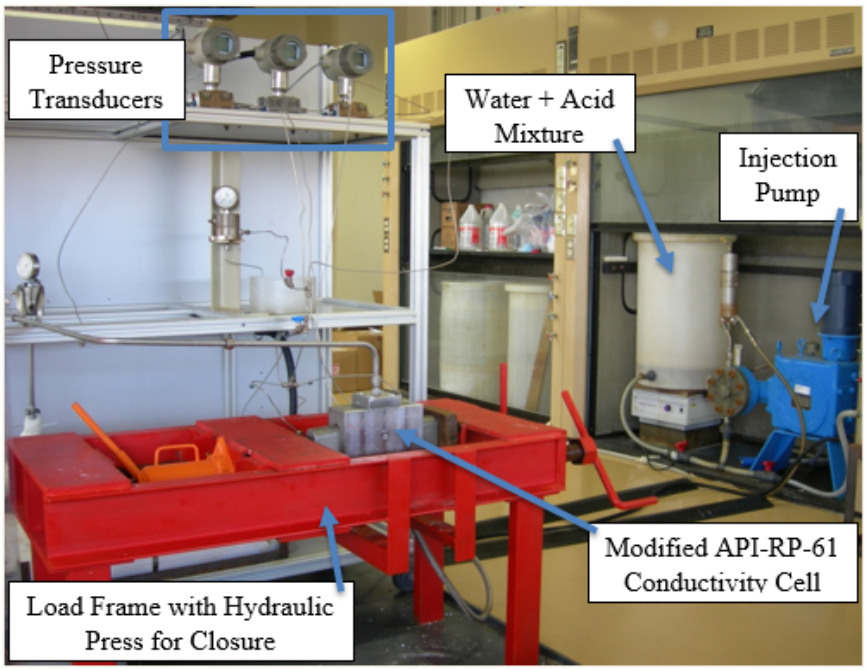

Fig. 8: Acid Fracturing Lab Setup

The sample is placed into the cell using a load frame. When placing the sample in the cell, the sample should be placed into the cell in a way that has the flow direction upwards. There should also be a fracture spacing of approximately 0.10 in. The two side pistons with O-rings on the edges are placed on the left and right of the cell prohibit the sample from moving during the test. In order to avoid gravity affects, the cell is placed vertically. The top and bottom flow inserts are where the fluid enters (bottom) and exits (top) the sample. A detailed laboratory setup for the acid fracturing experiments completed in this study is shown in **Fig. 9**.

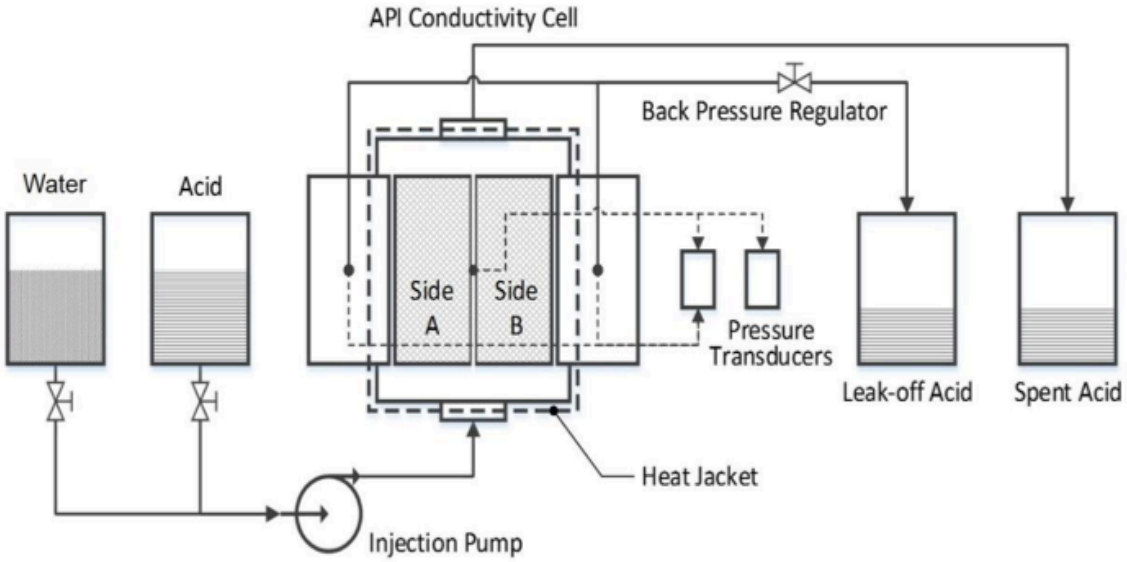

Fig. 9: Acid Fracturing Apparatus. Suleimenova, 2015.

After the cell has been placed into the load frame, the inlet and outlet valves are assembled. Two storage containers for the fluids are placed under the hood and connected to the system's pump with closing and opening valves. One container is for acid and the other is for water. Water is initially flowed through the system as a pre-flush and, after the acid, as a post-flush to establish a pH of at least 5. Using a pump allows the option of varying the injection rate from experiment to experiment. Injections rates can reach up to 1 liter/min and the flow rate can be set at 10-100% of its capacity. For this experiment, the flow rate is set at 1 liter/min. From the pump, the fluid flows through a braided stainless steel hose to the set-up, where the fluid enters the bottom of the API cell. Using a thermal heating jacket, the temperature of the cell can be set to the desired temperature.

There are three pressure transducers on the apparatus, one for cell pressure, one for leak-off differential, and one for fracture differential. Only cell pressure is monitored in this study. The leak-off valve in the apparatus is closed to block the measurement of leak-off differential. The upper and lower outlet ports on the API cell are plugged to block the measurement of fracture differential. The cell pressure is maintained at 1,000 psi to maintain the CO_2 byproduct from the acid in the solution. The leak-off regulator is closed since leak-off is not measured and all acid exits the system as spent acid. After the acid fracturing experiment is completed, the sample is removed from the mold, post scanned using the surface profilometer, and prepared for the conductivity experiment. The laboratory setup for the conductivity experiments completed in this study is shown in **Fig. 10**.

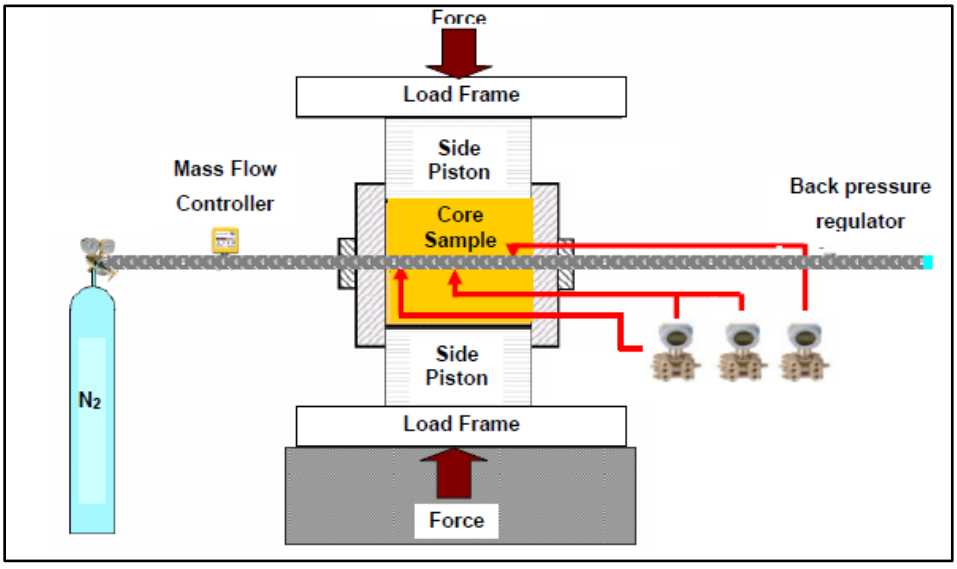

Fig. 10: Conductivity Laboratory Setup. From Melendez, 2007

After acidizing, to simulate fluid flow through a created fracture, nitrogen is flowed through a closed system at varying flow rates and the corresponding pressure drop is recorded under different closure stresses. A flowmeter is used to monitor the nitrogen flowing through the system and to vary the flowrates to obtain data. The sample is placed horizontally in a stainless steel API-RP-61 conductivity cell and then placed in a GCTS load frame testing system. The load frame can apply various amounts of pressure onto the system. For this study, the range of closure stress is from 500 psi. to 4000 psi, sample integrity permitting. 4000 psi was chosen as the upper closure stress for comparison of values to the study completed by Tripathi and Pournik (2014). The pressure drop across the system is recorded under four different flowrates for each closure stress value. From the recorded data, Darcy's Law for gas flow in porous media is used to obtain conductivity.

2.2 Experimental Procedure

There is a multi-step procedure needed to complete each individual experiment. The process is detailed in **Fig. 11**. Two additional tests are completed outside of the acid fracturing and fracture conductivity labs: Brinell Hardness Number, to determine sample hardness, and X-Ray Diffraction analysis, to estimate sample mineralogy.

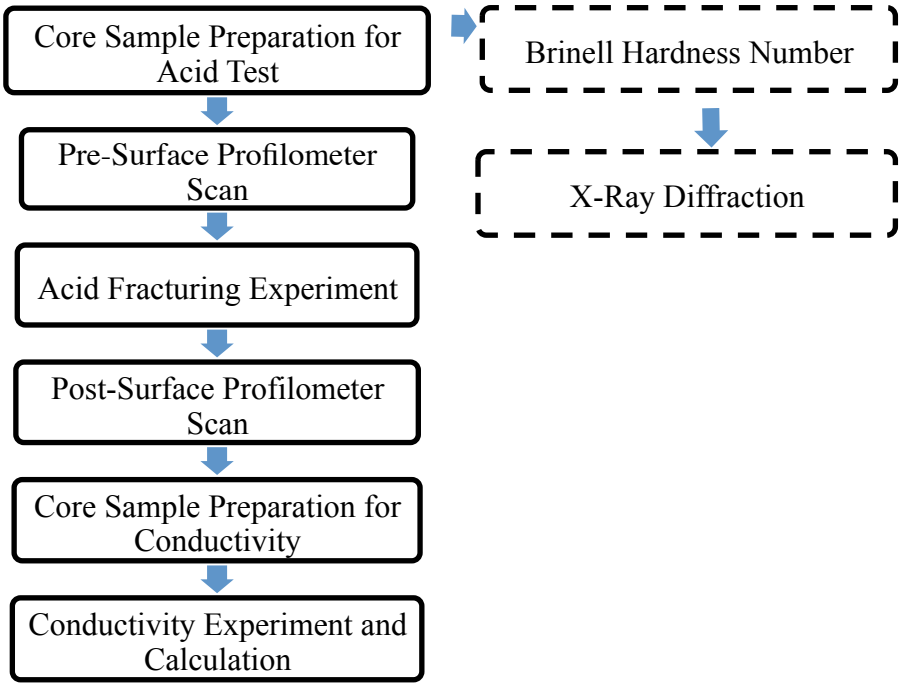

Fig. 11: Acid Fracturing Experimental Process

2.3 Core Sample Preparation

The core sample preparation used in this experiment is based on the work of Melendez (2007):

- The core samples are taped along the fracturing using contractor's masking tape to prevent epoxy from traveling into the fracture.
- The cutting direction (flow direction), left/right core halves, thickness in inches, and sample name are labeled to avoid ambiguity.

- The sides of the sample surface are sanded using minimally abrasive sandpaper.
- Silicon adhesive primer is next applied in three-fifteen minute intervals.
- The sample mold is cleaned using acetone and silicon mold release is applied. The mold release is applied in three-fifteen minute intervals.
- The sample is placed in the sample mold where silicone-potting compound is mixed and poured into the mold. The sample should be spaced evenly from all mold surfaces to ensure equal coating of the epoxy.
- The epoxy is slowly poured directly onto the top surface of sample and allowed to overflow the sample and down the annulus between the sample and mold wall. Overflow should ideally occur on the long edge of the sample, and preferably at just one location at first. The overflow should occurs at a slow enough rate to always see a gap between the flowing epoxy and the mold interior's top surface. As a rule of thumb, the pouring process should take ten to twenty minutes.
- The mold is placed in the drying oven for three to five hours and the sample is removed upon cooling.
- After sample and mold have cooled, the assembly is unscrewed, the sample is removed, and the mold is cleaned with acetone for the next use.
- The extra silicon remaining on the edges of the sample is cut with a razor cutter to create a clean edge around the sample.
- A pre-acid fracturing photo is taken of the sample to document physical sample characteristics.

2.4 Surface Characterization

Pre- and Post-surface scans are completed to obtain the total etched volume before and after acidizing. A surface profilometer, shown in **Fig. 12,** is used to determine the surface roughness created from acidizing. X-, Y-, and Z- coordinates are recorded in a text file, which is then uploaded into a pre-created Matlab program (Malagon, 2006). The surface profilometer uses a resolution of 0.05in for the X- and Y-coordinates and 0.001in for Z coordinates. Using the Matlab program, the total etched volume for the top and bottom surfaces of the sample is calculated.

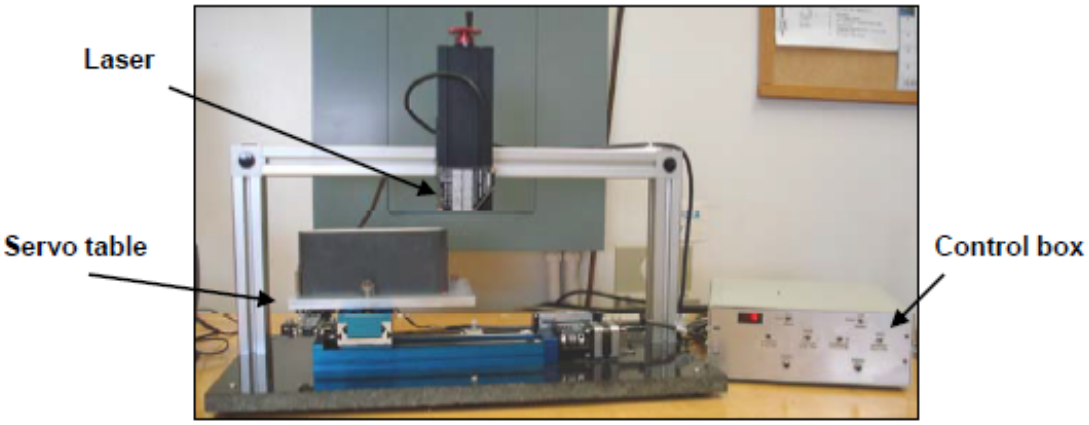

Fig 12: Profilometer setup. From Melendez, 2007.

2.5 Acid Etching

The procedure for the acid fracturing experiment is as follows:

- Using a vacuum pump, fill the sealable glass container connected to the vacuum pump with water.

- Place the left and right sample halves in the water and apply a thick layer of vacuum grease around the top edge of the container.
- Place the lid on the container. The system should immediately pressurize to around 25 psi. In the case that it does not, check to ensure the leak-off valve is closed. If this doesn't resolve the issue, shut off the vacuum pump, depressurize the system, remove the lid, and apply more vacuum grease.
- Monitor the system temperature every 10 minutes for the first 30 minutes to ensure that the system does not over heat. If the system reaches 50° C, shut down the vacuum pump and apply more vacuum grease. It is important to monitor the system so that it does not overheat.
- Allow the cores to saturate around three to four hours. If the cores are removed prior to testing, submerge them in water until the test is to be performed. This will allow the pores to remain opened.
- Clean the modified API-RP-61 conductivity cell using acetone.
- Apply a very thin layer of superglue around the two insets inside the mold and place an O-ring on each.
- Apply two layers of Teflon tape around the outside of each half of the sample.
- Place vacuum grease around where the tape was placed to help the sample slide into the mold.
- Place the cores inside the test cell using the load frame. Ensure that the cores are placed with the flow direction vertically upwards consistent with the flow direction of the acid.

- Push the cores into the mold, leaving a 0.10inch gap between the fractures. Do not allow the sides of each core to touch one another as this will cause problems in the acid fracturing system.
- Place the cell in the loading jack in the vertical position, placing the left and right side pistons into their spaces.
- Use the hydraulic jack to move the loading jack and press until the side pistons are in place.
- Using the load frame supports, ensure that the handles of the frame are turned clockwise until the cell is stabilized. This acts as a secondary support to hold the cell in place during the experiment. Also place two C-clamps on the left and right sides of the two springs on the load frame for extra stability.
- Once the cell is stabilized, connect the lines for the pressure sensors. The outlet line for the system should be placed where that the fluid will flow into a waste approved container.
- After all lines have been attached, perform a secondary check to ensure that all lines are properly connected prior to introducing fluid to the system.
- Turn the pump on, open the water line, and monitor the system to make sure there are no leaks. In the case that there is a leak, shut off the water source, determine the source and tighten the connection. If this does not resolve the problem, the end fittings may have to be replaced due to broken threads in the connection.

- The pump injection rate can be set up to 1.0L/min. The flow rate can be set manually by turning the back cylinder of the pump clockwise, which is shown in **Fig. 13**.

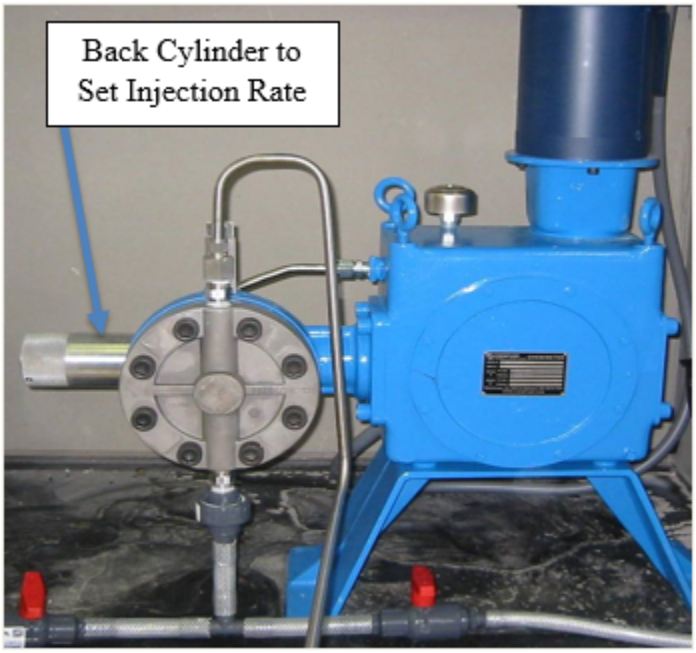

Fig 13: Chem/Meter 800 Series Pump

- Turn on the nitrogen and allow it to flow through the system. Slowly increase the nitrogen amount to ensure there are no leaks as you increase cell pressure.
- The cell pressure is maintained at 1,000 psi to maintain the CO_2 byproduct of the acid reaction. The leak-off differential and fracture differential pressure transducers are not used in this experiment.
- Check the system again for leaks. If there are leaks, depressurize the system, shut off the water source, and tighten the connection where the leak is found.

- If the thermal heating jacket is needed, turn it on and set the upper temperature limit.
- Once the system is correctly running with no leaks, the desired temperature has been reached, and the pressure is maintained, set the pump to the desired output.
- Next, prepare the acid. Depending on experimental requirements, different acid components, such as corrosion inhibitor and gelling agents may be added. For this experiment, 36 molar HCl is used and diluted to the desired HCl concentration. Always mix acid into water since burns can result from released heat during the addition.
- The acid-water mixture is mixed using a magnetic mixer.
- Move the water outlet hose from the sink to an approved acid waste barrel.
- Open the brine line and close the water line. Flow the acid through the system the desired contact time.
- After the acid contact time is reached, turn close the brine line and open the water line. Keep the outlet valve in the acid waste container until the system has been flushed.
- Once a pH of 5 or greater is reached, it is safe to move the outlet hose back to the sink.
- Check for any acid leakage. In the case that acid has leaked from the system, apply acid neutralizer to the affected areas. The acid neutralizer will change colors when the pH of the leak is at a safe level.

- Turn off the heater (if used) and depressurize the system. Always depressurize the system before removing any lines. Ensure all pressure is discharged from system by reading cell pressure transduced value, which should read less than 0.20 psi prior to disassembling the equipment.
- Turn off the pump and close the water flow line.
- Remove all lines from the system and remove the cell from the load jack by turning the ends of the load frame counterclockwise and releasing the hydraulic jack.
- Using a hydraulic press, carefully remove the sample from the cell. Wipe off any residue from the outside of the sample.
- Clean the cell with acetone, completely removing the 2 inside O-rings.
- Using the surface profilometer, scan the left and right sides of the sample. With the before-acid and after-acid scans, the total etched volume can be calculated using a created Matlab program.
- A post-acid fracturing photo is taken of the sample to document physical sample characteristics.

2.6 Acid Fracture Conductivity Measurement and Calculation

The procedure for the acid fracture conductivity experiment is based on the work of McGinley (2015) and is as follows:

- Remove the epoxy that was applied to the sample for the acid fracturing test.
- Clean the API-RP-61 conductivity cell with acetone to ensure that all residue is removed.

- Re-prepare the sample with epoxy for use in the conductivity experiment. Cut three squares, roughly 2cm x 2cm, at approximately 3cm, 9cm, and 15cm along the horizontal side of the sample where the pressure ports are located. This allows the pressure transducers access into the sample. The squares should be cut along the left side of the sample where the three access ports are located on the cell, with the flow direction facing toward the person placing the sample into the cell.
- Wrap the sample horizontally approximately two times with Teflon tape 1.5" above and 1.5" below the pressure port holes. Wrap the sample vertically approximately two times with Teflon tape halfway between the outer and middle pressure ports.
- Apply high vacuum grease to the Teflon taped areas.
- Place the sample into the API-RP-61 conductivity cell using a hydraulic press. It is important to correctly place the sample into the cell with the corresponding flow direction as this helps ensure more realistic results.
- Using a small screwdriver, check to make sure the cut squares are in contact with the pressure transducers. Exposed rock will make a different sound than epoxy.
- Apply a thin layer of O-ring grease to the O-rings on each of the two side pistons. If the O-rings are broken, place new O-rings on the pistons.
- Place two layers of Teflon tape along the O-rings on the two side pistons. This helps prevent leakage in the system.

- Place the two side pistons onto the cell. If the pistons aren't all the way pressed into the cell, the load frame will push the pistons into the cell when the GCTS system applies closure stress.
- Place the stabilizer sleeve around the bottom side piston and tighten the bottom piston's bleed port bolt. To help decrease leakage, wrap the bolt with two layers of Teflon tape prior to tightening it.
- Move the cell onto the GCTS frame, placing the cell in the center of the system to ensure an even distribution of force onto the sample.
- Turn on the GCTS UCT-1000 control box. After the control box shows only green lights, open the corresponding GCTS software.
- Plug in the Aalborg mass flowmeter, allowing the reading to stabilize.
- In the GCTS software, turn on the pump and create a new test sample file.
- Attach the upstream and downstream pressure transducers, with the wiring exiting the bottom portion of the transducer. If the wiring is attached upwards, the pressure readings will be negative.
- Secure the mold holder end caps using four screws for each side.
- Attach the gas flow inlet and outlet lines to the mold holder end caps. Do not use Teflon tape on these connections as it will break the threads on the tubing fittings.
- Tighten the top bleed port bolt. To help decrease leakage, wrap the bolt with two layers of Teflon tape prior to tightening it.

- Before opening the nitrogen valve, ensure that the tank regulator, gas backflow valve and gas inlet bleed valve are closed. The only valve that should be open is the gas inlet valve.
- Open the nitrogen valve and slowly open the regulator valve, adjusting the system pressure to approximately 30 psi. Using the proper diaphragm for the pressure transducer, the system can only be calibrated up to 30 psi, therefore the system should not be set above this value.
- As the nitrogen begins to flow through the valve, do not allow the flow to reach 10 L/min as this is the maximum reading for the flow meter.
- The reading on the flow meter should stabilize. If it does not stabilize, the system has a leak. Using a mixture of soap and water, squirt the mixture along the connection in the system to find the leak. Once the leak is found, tighten the connection if necessary.
- Closure stress is applied initially as 500 psi, then 1000 psi and in increments of 1000 psi after that. The maximum closure stress used is 8000 psi, above which the sample can be greatly damaged.
- After the system has reached 500 psi, open the backflow valve at increasing levels to take four readings. The four readings should be taken at values of 20%, 40%, 60%, and 80% of the rated diaphragm value. Each measurement point has the following requirements:
    - -Differential pressures must be 0.4-1.6 psi
    - -Cell pressure must be 28-30 psi due to pressure transducer calibration

- -Recorded flow rates should be different at each reading (more than 0.05 L/min difference)

- Record the four flow rates and corresponding system pressure and enter into the created fracture conductivity Excel spreadsheet.
- Repeat the flow measurements to the desired closure stress.
- After the experiment is completed, close off the nitrogen tank root valve.
- Slowly open the inlet bleed valve to release the nitrogen. Monitor the flow meter to make sure the flow does not exceed 10 L/min.
- After the system is depressurized, disassemble the flow lines and mold holder end caps.
- Set the GCTS computer program to "Axial Displacement" to move up the uniaxial compression system so that the cell can be removed from the testing frame.
- Remove the top and bottom side pistons and carefully remove the sample using a hydraulic press.
- Turn off the pump and close the GCTS software and controller box.
- Clean both side pistons and the conductivity cell with acetone to remove any remaining residue.
- Using the recorded pressure drop values for each closure stress, conductivity is calculated using Darcy's law for gas flow in porous media shown in **Eq. 3**.

$$\frac{(p_1{}^2-p_2{}^2)M}{2ZRTL} = \frac{1}{wk_f}\frac{\mu\rho q}{h} \quad \text{.....(eq. 3)}$$

The pressure squared difference is measured in the lab at four different flowrates under differing closure stresses. The other variable values used are shown in **Table 1**.

Table 1: Variables Used for Conductivity Calculations

Variable	Meaning	Units	Value
M	Molecular mass of nitrogen	kg/kg mol	0.028
h	Height of fracture face	in	1.75
Z	Compressibility factor	N/A	1.00
R	Universal constant	J/mol K	8.32
L	Length of fracture over which pressure drop is measured	in	5.25
μ	Viscosity of nitrogen at standard conditions	Pa.s	1.747E-05
ρ	Density of nitrogen at standard conditions	kg/m^3	1.16085
T	Room temperature	K	293.15

2.7 Experimental Conditions

Constant parameters for all experiments in this study include 0.1" fracture width, 1000 psi cell pressure during acid fracturing experiments, and a closure stress of up to 4000 psi for conductivity tests, sample integrity permitting. The dependent variables were contact time, temperature, and HCl concentration. Three test conditions shown in **Table 2** were used: test condition #1, #2 and test condition #3, with the latter being completed for a comparison between the Tripathi and Pournik 2014 study.

Table 2: Experimental Test Conditions

Test Condition	HCl Concentration	Acid Contact Time	Temperature
1	28wt.%	20 minutes	190°F
2	15wt.%	20 minutes	190°F
3	15wt.%	10 minutes	Ambient

Using the test conditions described in **Table 2**, eight total samples were tested, shown in **Table 3**.

Table 3: Test Conditions used for each Sample

Test Condition	Zone	Sample Name
1	C	EF_C_1
		EF_C_2
	D	EF_D_1
		EF_D_2
2	C	EF_C_3
	D	EF_D_3
3	C	EF_C_4
	D	EF_D_4

Eight total samples were tested: four at test condition #1 with two samples from zone C and D, two at test condition #2 with one sample from zone C and D, and two at

test condition #3 with one sample from zone C and D. The change in vertical depth, or total surface etching volume was calculated by pre- and post-acidizing surface profilometer scans.

CHAPTER III

EXPERIMENTAL RESULTS AND DISCUSSION

3.1 Case Study Background

In this study, eight Eagle Ford shale samples, four from each zones C and D are used to test the effects of acid fracturing. The Eagle Ford shale formation was deposited above the Buda limestone formation and below the Austin Chalk formation. The Eagle Ford shale is divided into zones A-E of characterization, originally determined by Donovan and Staerker (2010), as shown in **Fig. 14**. Sample rocks used in this study are outcrop rocks from Terrell County, Texas from the Upper Eagle Ford Formation zones C and D, shown in **Fig. 15**. The Upper Eagle Ford contains two members, the Langtry and Scott Ranch members.

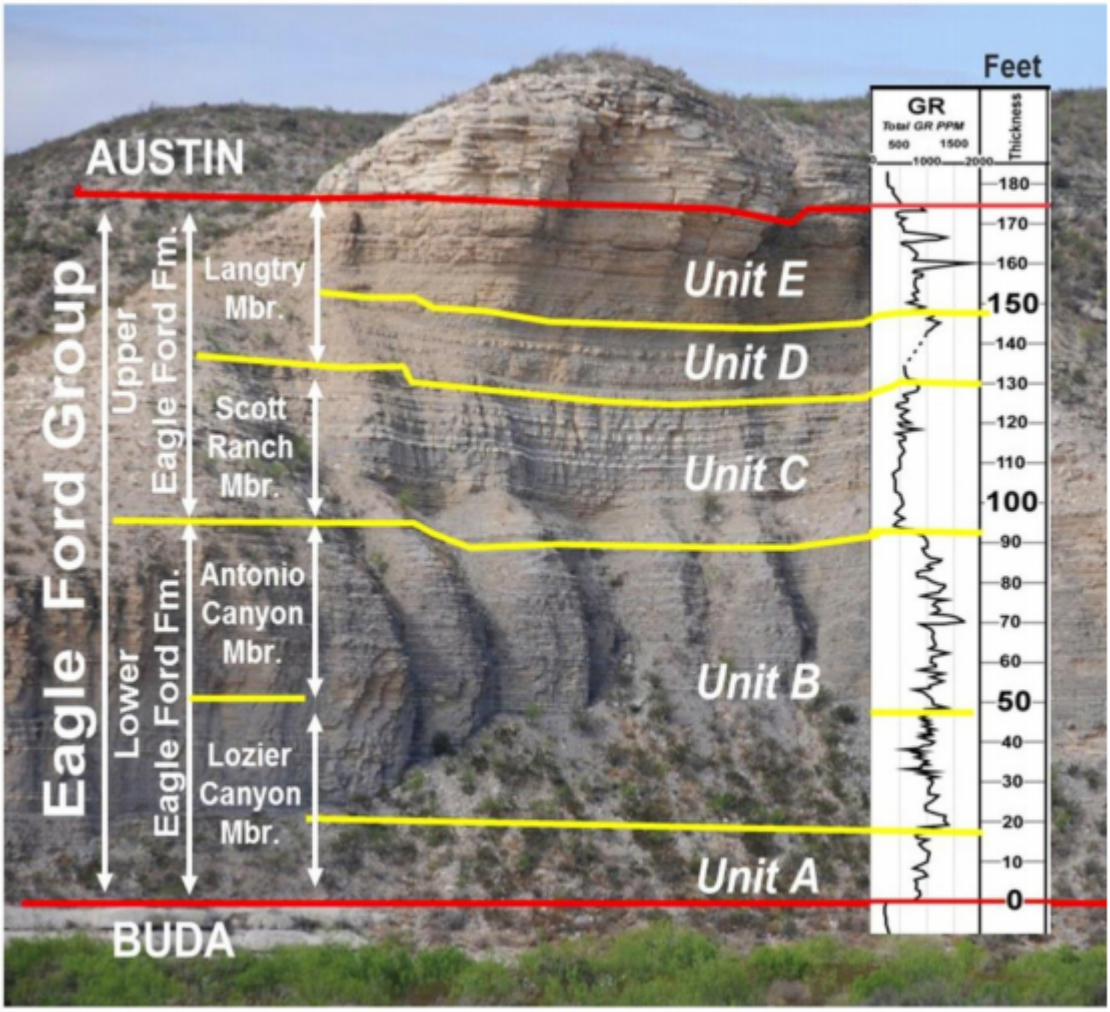

Fig 14: Zones of the Eagle Ford Shale with Corresponding Gamma Ray Response at the Lozier Canyon BP Field Site. From Donovan et al., 2012.

Due to the oxic nature of the Upper Eagle Ford, production in the Eagle Ford formation is predominately from zone B, the area of highest gamma ray response. However, due to sample availability, only samples from zones C and D were tested. There is a high calcite content throughout the Eagle Ford formation resulting from carbonate platform developed during the Early Cretaceous and earliest Late Cretaceous periods, named the Comanche Platform (Gardner et al., 2013).

The potential success of acid fracturing the Eagle Ford shale is dependent upon the formation characteristics, specifically the carbonate content. Classification in the Gardner et al. (2013) study is based on Dunham's classification (1962) for Carbonate rocks and Campbell's classification (1967) for sedimentary structures. Zone C is approximately 40-ft of skeletal wackestone-packstone interbedded with dark gray calcareous mudstone, sans thick bentonite beds potentially due to the erosional surfaces common in calcareous mudstones. Zone D is approximately 20-ft thick consisting of nodular skeletal packstone interbedded with medium gray calcareous mudstone, with thin layers of bentonites.

Zone	C	D
Average Thickness	40.5 ft.	20.5 ft.
Lithology	Medium gray calcareous mudstone interbedded with 2-12 in. thick bed sets of skeletal wackestone-packstone; thin <1 in. thick bentonite beds; abundant forams, bivalves, pellets, frambroidal pyrite	1-8 in. thick irregular layers and nodules of skeletal wackestone and packstone; bedding is burrow homogenized; interbedded calcareous mudstone; thin <1 in. thick bentonite beds; abundant fossils such as bivalves and brachiopods, frambroidal pyrite
Sedimentary Structures	Abundant burrows, cross laminations, low-angle inclined laminates, ripple laminations	Abundant burrows; rare preserved cross stratified laminates in nodules
Depositional Environment	Open shelf within storm wave base; oxic	Open shelf within storm wave base; oxic

Fig. 15: Location of Sample Obtainment (left) and Description of Zones C and D of the Eagle Ford Shale. Modified from Gardner et al., 2013.

Zone B is the present area of production in the Eagle Ford shale due to its anoxic depositional environment, within a restricted shelf and somewhat periodically in a storm wave base. Both zones C and D have oxic depositional environments due to the increase in bioturbation and decrease in Uranium prevalent in the Upper Eagle Ford formation. Gardner et al. determined that zones A, C, D, and E in the Eagle Ford were originally deposited above the storm wave base in relatively shallow water from a sedimentary structure study.

3.2 Sample Description

Applying the classification in the Gardner et al. study, based on Dunham's classification (1962) for Carbonate rocks and Campbell's classification (1967) for sedimentary structures, a description for each sample used in this study is given in **Table 4**. Hardness values were not obtained for samples EF_C_4 or EF_D_4, as those samples were used solely for comparison to the Tripathi and Pournik (2014) study.

Table 4: Description of Eagle Ford Samples from Current Study

Sample	Lithology	Sedimentary Structures	Depositional Environment	Calcite Content (XRD Analysis)	Brinell Hardness Kg-f/mm^2
EF_C_1	Medium gray calcareous mudstone interbedded with wackestone and packstone	Cross and ripple laminations	Open shelf within storm wave base; oxic	75%	84
EF_C_2					71
EF_C_3					85
EF_C_4					N/A
EF_D_1	Interbedded calcareous mudstone with wackestone and packstone	Cross and ripple laminations	Open shelf within storm wave base; oxic	83%	102
EF_D_2					115
EF_D_3					102
EF_D_4					N/A

3.3 Results for Test Conditions #1 and #2

The total dissolved surface etching volume for the six Eagle Ford samples with corresponding acid fracture conductivity values are shown in **Table 5.**

Table 5: Total Left and Right Etching Volumes (in^3)

Sample	Test Condition	Left Etching Volume (in^3)	Right Etching Volume (in^3)	Conductivity (md-ft) Resulting from Closure Stress				
				500 psi	1000 psi	2000 psi	3000 psi	4000 psi
EF_C_1	1	0.113	0.264	1010	976	443	132	9
EF_C_2	1	0.097	0.065	806	444	227	69	10
EF_C_3	2	0.081	0.138	491	242	45	41	20
EF_D_1	1	0.033	0.004	18	17	12	22	-
EF_D_2	1	0.320	0.440	1092	825	150	76	50
EF_D_3	2	0.710	0.785	920	901	403	89	70

The surface etching pattern, surface etching volume, and resulting conductivity are further discussed for each of the samples listed in Table 5. Each sample will be analyzed as having a left side and a right side. Together, the left and right sides constitute one sample.

3.3.1 EF_C_1

Sample EF_C_1 was tested with 28wt% HCl for 20 minutes and the resulting surface etching patterns are shown in **Fig. 16**.The right core had some visible striations near the center of the core. The sample experienced a lower etching pattern of

channeling to roughness, with channeling in the y-direction. The total dissolved etching volume for the right side was 0.264in^3. Channeling is normally present in the x-direction, however the channeling occurred along the path of the striations.

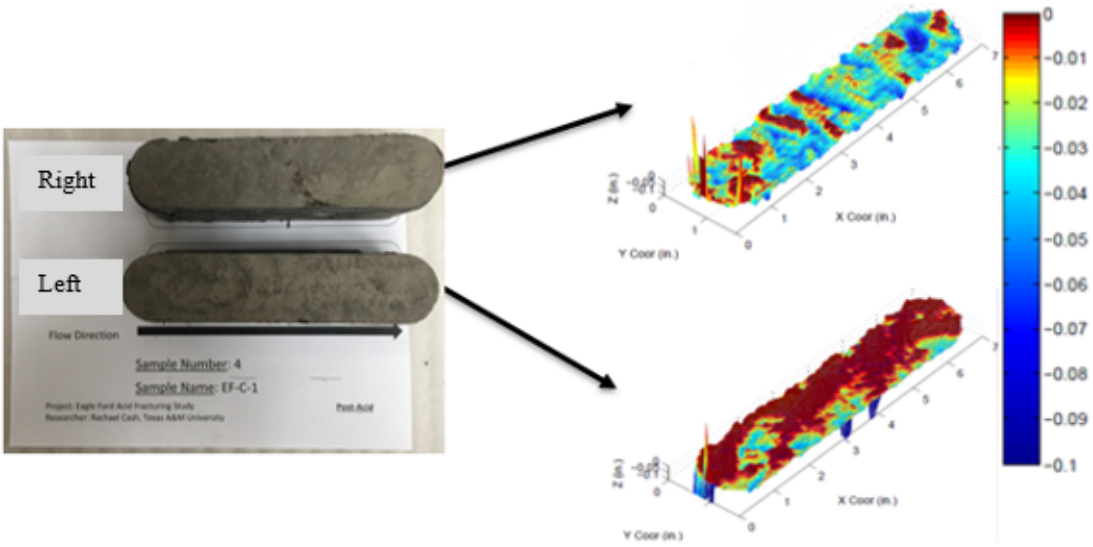

Fig. 16: Post Sample Surface Image and Difference in Surface Profile of EF_C_1. Right and Left Etching Volumes are 0.264 in^3 and 0.113 in^3 respectfully.

The left side of the sample had minimal roughness along the right edge of the sample to a non-etching pattern. The areas of red on the right core acted as barriers, closing off the pathway of the acid along the left core. This acid was then diverted along the right side of the left core, where the majority of etching occurred on the left core, creating a total dissolved etching volume of 0.113in^3.

The channeling to roughness etching pattern of the right core created a high initial conductivity of 1010mD-ft, shown in **Fig. 17**. The conductivity was sustained by

the created channels up to 3000psi of closure stress, after which a sharp decline was experienced. Due to the non-etching of the left core, there were insufficient surface asperities to help the fracture remain completely opened. The ending conductivity for the sample was 9mD-ft.

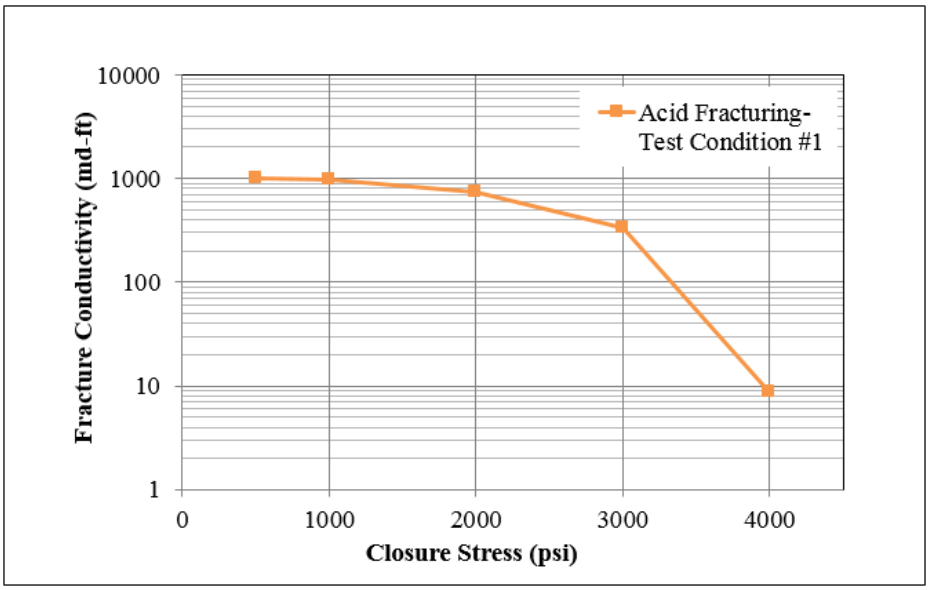

Closure Stress (psi)	k_f-w (md-ft)
500	1010
1000	976
2000	729
3000	332
4000	9

Fig. 17: Acid Fracture Conductivity for EF_C_1

3.3.2 EF_C_2

Sample EF_C_2 was tested with 28wt% HCl for 20 minutes. Corresponding surface etching results are shown in **Fig. 18**. The right core experienced a non-etching pattern resulting in an etching volume of 0.065in^3, with the highest volume of etching occurring along the darker colored vein-like region in the sample. This resulted in the yellow and orange color on the surface scan results in Fig. 18.

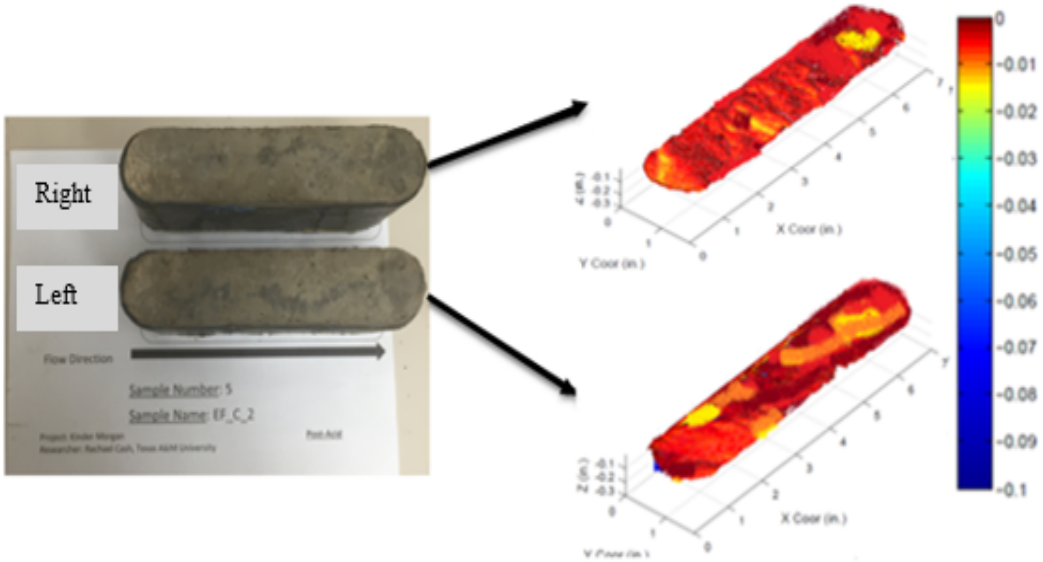

Fig. 18: Post Sample Surface Image and Difference in Surface Profile of EF_C_2. Right and Left Etching Volumes are 0.065 in^3 and 0.097 in^3 respectfully.

The left core also had non-etching, with the highest degree of etching occurring along the darker colored vein-like region. The total surface etching volume of the left core was 0.097in^3. The lack of surface etching for EF_C_2 is most likely due to the lower calcite content of zone C. Due to the high heterogeneity of the Eagle Ford shale,

the composition of the outcrop rock from which all zone C samples were taken could vary sample to sample. EF_C_1 had higher etching volumes than EF_C_2, which can be explained by a difference in minerals dissolvable by HCl.

Although the sample did not experience a high degree of surface etching, the initial conductivity was still significant at 806mD-ft, as shown in **Fig. 19**. As closure stress increased, there was a decline approximately one-half the previous conductivity value, up until 3000 psi. As closure stress increased past 2000 psi, the sample sharply declined, unable to support the opened fracture. Although the sample overall did not experience a high degree of etching, the etching of the sample along the darker colored vein-like region along the left and right cores provided a flow path that was able to stay minimally opened under increasing closure stress, ending with an acid-fracture conductivity of 10 mD-ft.

Closure Stress (psi)	k_f-w (md-ft)
500	806
1000	444
2000	227
3000	69
4000	10

Fig. 19: Acid Fracture Conductivity for EF_C_2

3.3.3 EF_C_3

Sample EF_C_3 was tested with 15wt% HCl for a contact time of 20 minutes. **Fig. 20** shows the resulting surface etching volumes for the right and left cores. The right core half had a non-etching pattern with a total dissolved etching volume of 0.082in^3. The left core had minor channeling to a non-etching pattern of 0.138in^3, with the channel present along the left side of the core. Any injected acid will follow the path of least

resistance in a formation, therefore it is reasonable to conclude that calcite was present on the left core where the channel was formed. The total surface etching volumes of both right and left cores is also a result of the lower concentration of 15wt% HCl used, as compared to the 28wt% HCl.

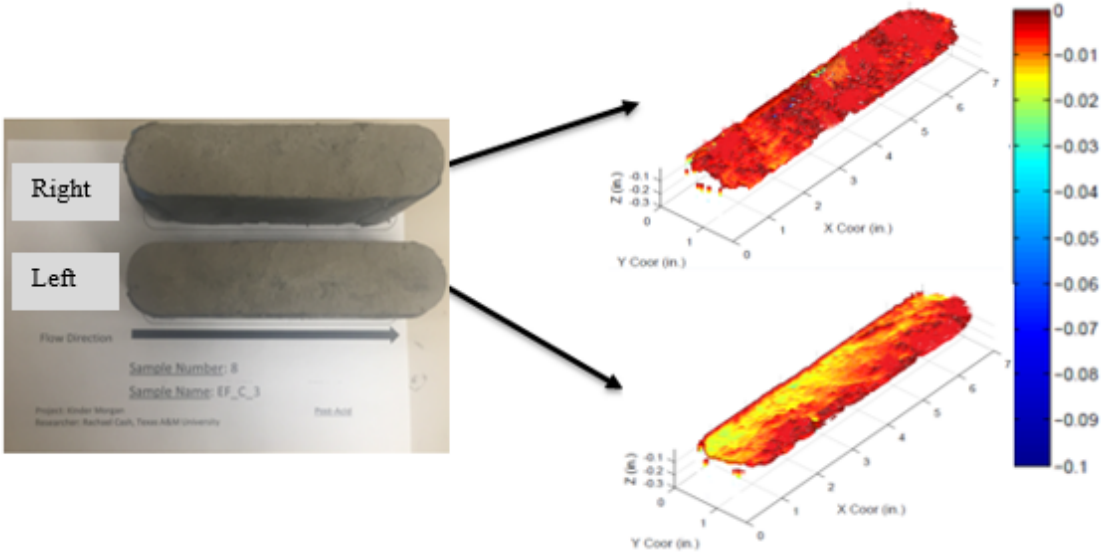

Fig. 20: Post Sample Surface Image and Difference in Surface Profile of EF_C_3. Right and Left Etching Volumes are 0.082 in^3 and 0.138 in^3 respectfully.

Initial acid fracture conductivity of C_3 was low in comparison to EF_C_1 and EF_C_2. Due to the smaller degree of surface etching, the conductivity sharply declined as closure stress increased up to 2000 psi, which is shown in **Fig. 21**. After this point, there was a gradual decline in conductivity with increasing closure stress. The 15wt% HCl did not weaken the fracture to face to the point that it was unable to remain opened

and ended with a conductivity of 20mD-ft. Sample EF_C_3 sustained conductivity at a higher ending value than EF_C_1 and EF_C_2.

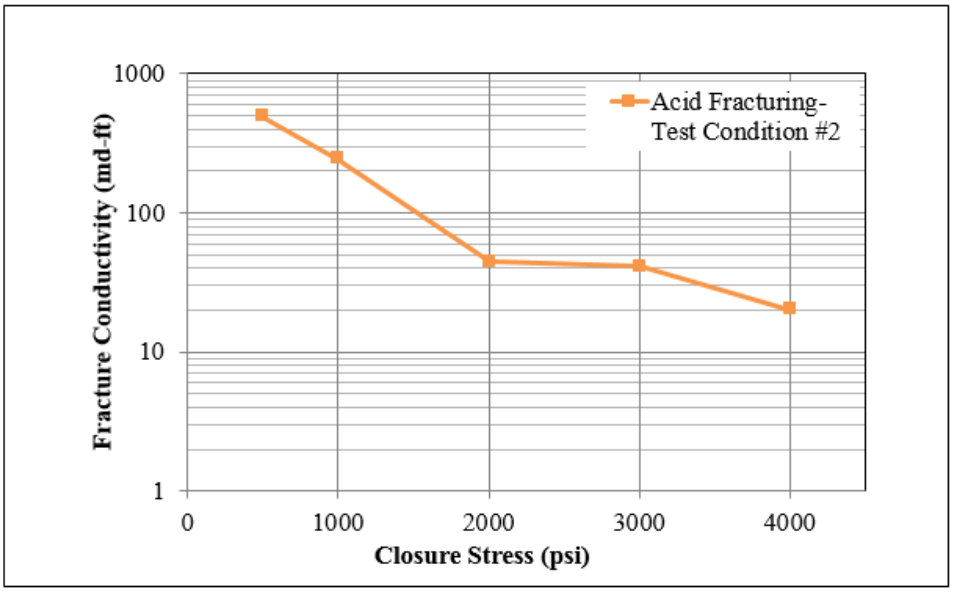

Closure Stress (psi)	k_f-w (md-ft)
500	491
1000	242
2000	45
3000	42
4000	20

Fig. 21: Acid Fracture Conductivity for EF_C_3

3.3.4 Comparison of Zone C Results

For zone C, EF_C_1 and EF_C_2 initially had higher conductivity values compared to EF_C_3, shown in **Fig. 22**. At 3000 psi, EF_C_1 and EF_C_2 experienced

sharp declines in conductivity. EF_C_3 was able to sustain fracture conductivity at a higher rate.

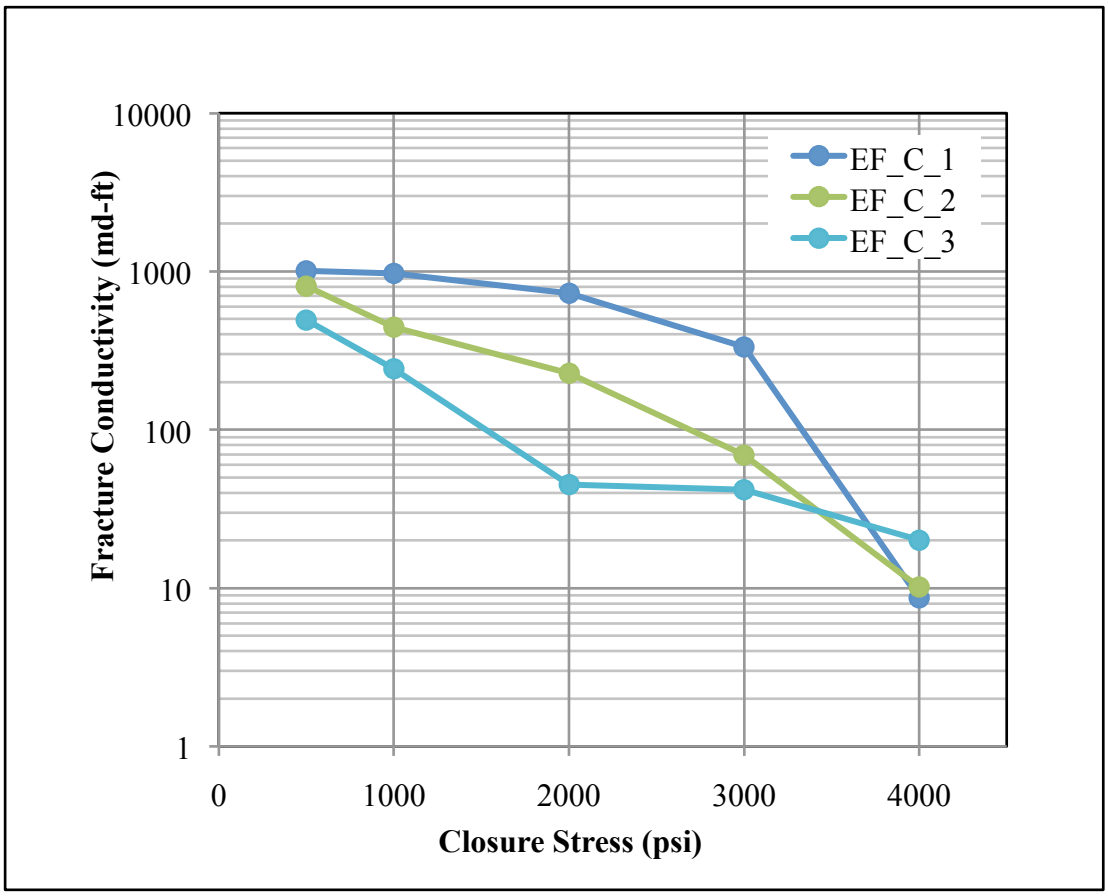

Fig. 22: Acid Fracture Conductivity for EF_C_3

3.3.5 EF_D_1

Sample EF_D_1 was tested with 28wt% HCl for 20 minutes. **Fig. 23** shows the resulting etching pattern for the right core as non-etching with minor roughness at the right end of the sample. The total etching volume for the right core was 0.004in^3. The etching pattern for the left core was roughness, with one cavity in the center of the core, for an etching volume of 0.033in^3.

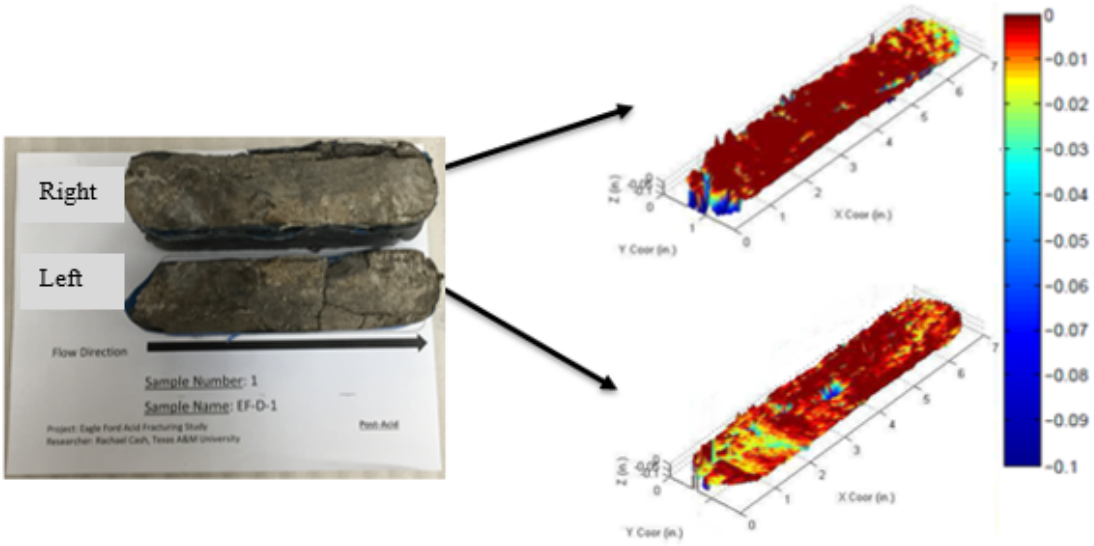

Fig. 23: Post Sample Surface Image and Difference in Surface Profile of EF_D_1. Right and Left Etching Volumes are 0.004 in^3 and 0.03 $3in^3$ respectfully.

Sample EF_D_1 broke during the conductivity test as closure stress increased from 2000 psi to 3000 psi. The conductivity test results are shown in **Fig. 24**. The increase in conductivity at a closure stress of 3000 psi represents loss of sample integrity, which is why the experiment was not continued to 4000 psi. Upon sample removal and inspection, it was noted that the sample was crushed during the application of additional closure stress. The original location of the cavity in the post-acid profilometer results was in the location of the initial point of rock breakage on the left core. The 28wt% HCl propagated into the rock through the cavity, weakening the rock to the point of breakage.

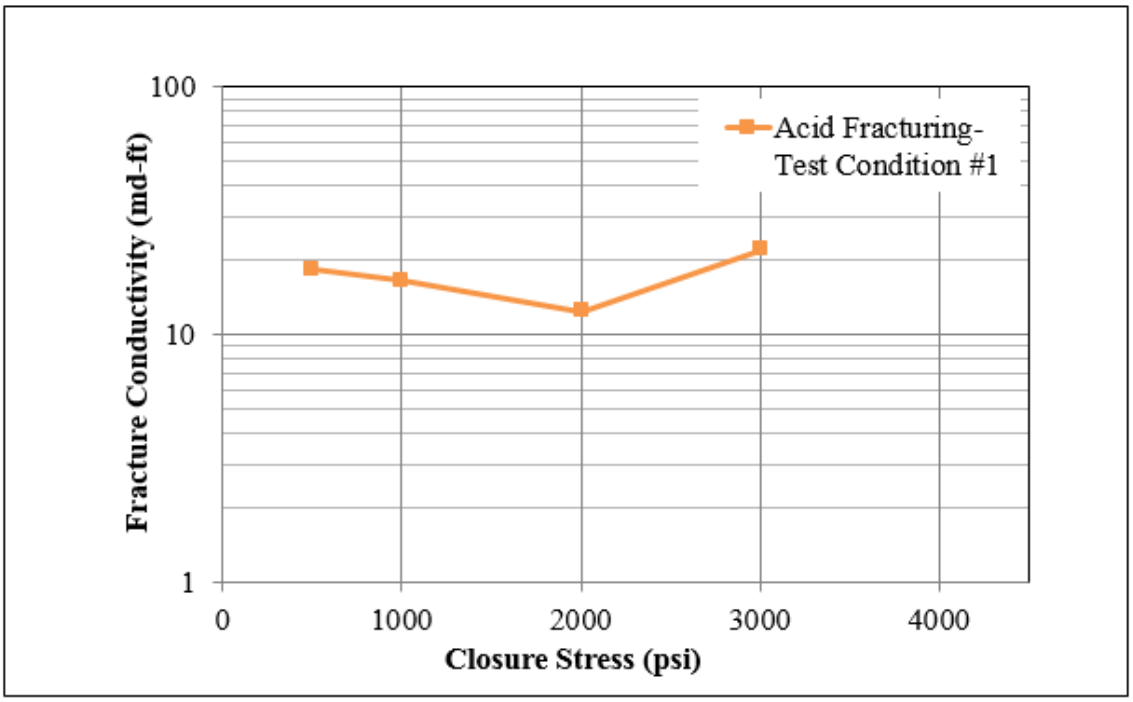

Closure Stress (psi)	k_f-w (md-ft)
500	18
1000	17
2000	12
3000	22
4000	-

Fig. 24: Acid Fracture Conductivity for EF_D_1

EF_D_1 results should not be considered to reflect the overall trends observed from zone D samples; experimental errors occurred in the acid fracturing experiment in addition to the rock breaking during the conductivity experiment. Errors that occurred during the acid fracturing experiment were improper fracture width between the left and

right cores in the modified conductivity cell, which decreased the amount of acid that was able to flow between the samples.

3.3.6 EF_D_2

Sample EF_D_2 was tested using 28wt% HCl and a 20 minute contact time and the surface profile is shown in **Fig. 25**. Dominant channeling was present on the right core, with some turbulent etching on the left side. Two major channels were present (shown in royal blue) on the right area and center of the core. The right core etching volume was 0.144in^3. The left core also experienced dominant channeling to turbulent etching patterns, with one major channel formed in the center of the core. The left core had an etching volume of 0.320in^3.

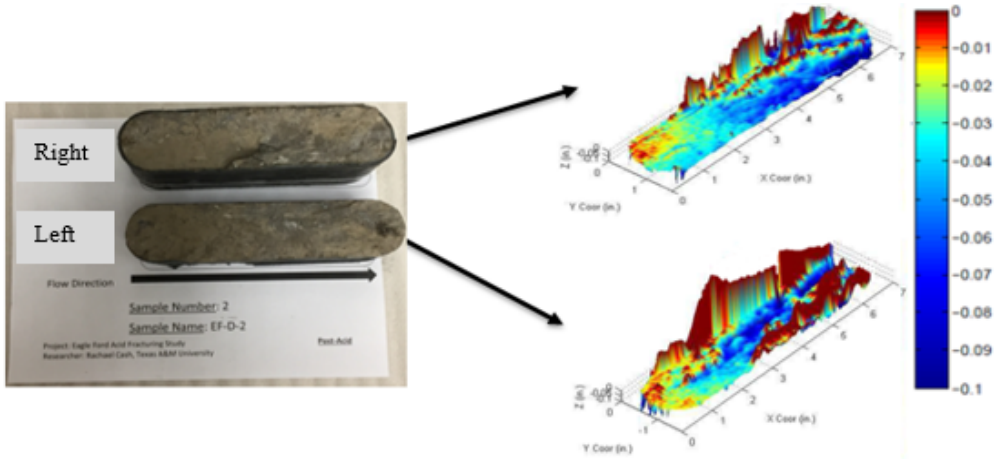

Fig. 25: Post Sample Surface Image and Difference in Surface Profile of EF_D_2.

Right and Left Etching Volumes are 0.144 in^3 and 0.320 in^3 respectfully.

The dominant channeling surface etching created a high initial conductivity value of 1092 md-ft, which is shown in **Fig. 26**. After 1000 psi, the sample experienced rapid decline in conductivity from 824 md-ft to 150 md-ft at 2000 psi. This decline is due to

the more turbulent etching pattern on the right core, which caused failure in some of the surface asperities on the sample. However, due to the dominant channel etching pattern, the created fracture was able to remain open, ending with the second highest conductivity value of the six samples at 50 md-ft.

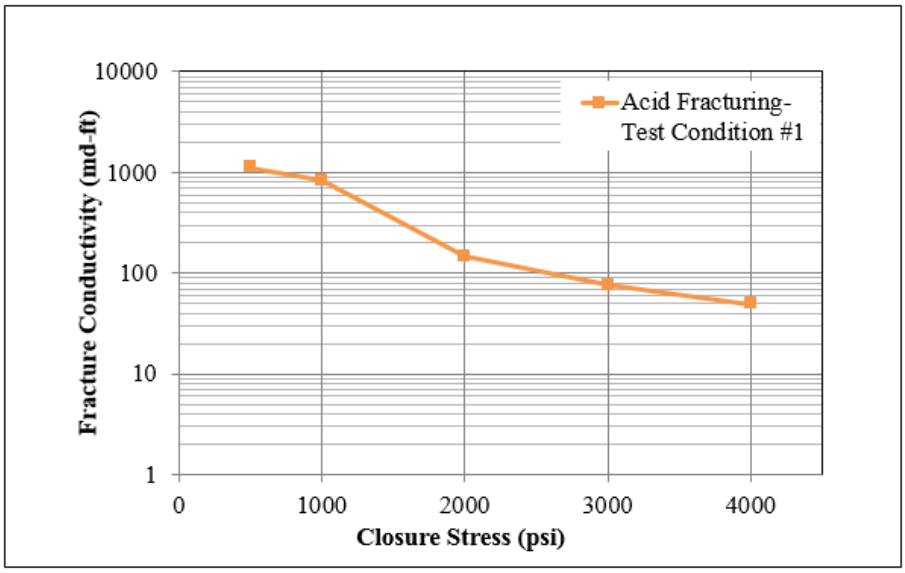

Closure Stress (psi)	k_f-w (md-ft)
500	1093
1000	825
2000	150
3000	76
4000	50

Fig. 26: Acid Fracture Conductivity for EF_D_2

3.3.7 EF_D_3

EF_D_3 was tested under test condition #2: 15wt% HCl for 20 minutes. The surface etching results are shown in **Fig. 27**. The right and left cores both experienced dominant channeling to roughness etching patterns, with total dissolved etching volumes of 0.785in^3 and 0.720in^3, respectively. This was the highest degree of surface etching of all experiments. This is most likely a result of the high calcite content in sample D_3. In Fig. 27, the rock sample appears visually to have more Austin Chalk sample characteristics. On the right end of each of the sample sides, there is a darker colored area, which is reflected in the surface etching results as yellow to reddish areas of less etching. Presumably, these areas have less calcite present.

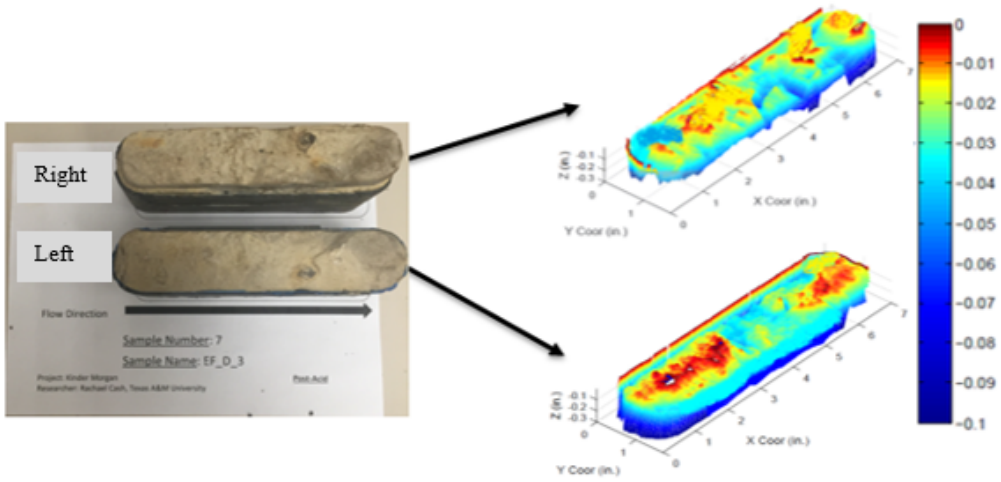

Fig. 27: Post Sample Surface Image and Difference in Surface Profile of EF_D_3. Right and Left Etching Volumes are 0.785 in^3 and 0.720 in^3 respectfully.

The dominant channeling etching pattern created very high initial conductivity and the sample was able to retain fracture conductivity, ending with a conductivity of

70mD-ft at 4000 psi closure stress, as shown in **Fig. 28**. This was the highest ending conductivity value of all samples tested. The reason for the high ending conductivity is due to the lack of weakening of the rock face from 15wt% HCl. The surface asperities were able to support additional closure stress at a higher rate than the other zone D samples tested with 28wt% HCl.

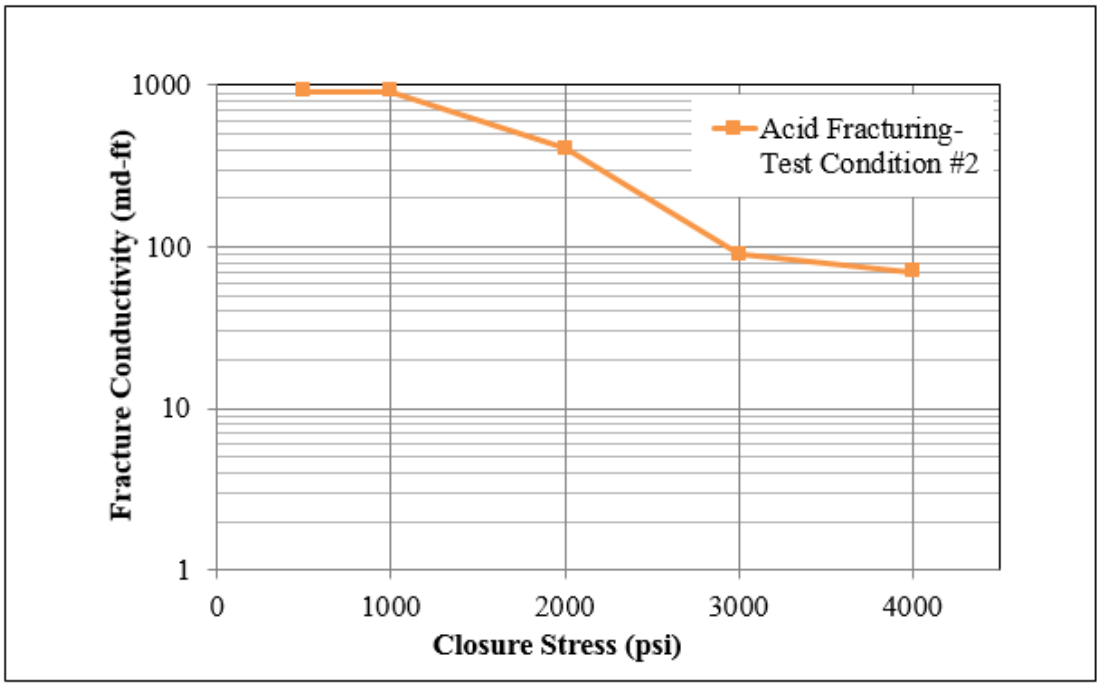

Closure Stress (psi)	k_f-w (md-ft)
500	920
1000	901
2000	403
3000	89
4000	70

Fig. 28: Acid Fracture Conductivity for EF_D_3

3.3.8 Comparison of Zone D Results

Considering EF_D_1 as an outlier, EF_D_2 and EF_D_3 samples started with approximately equal conductivity, shown in **Fig. 29**. Both latter samples experienced a decline, with EF_D_2 having a higher decline at 2000 psi. EF_D_3 was able to sustain fracture conductivity at a higher rate than EF_D_2.

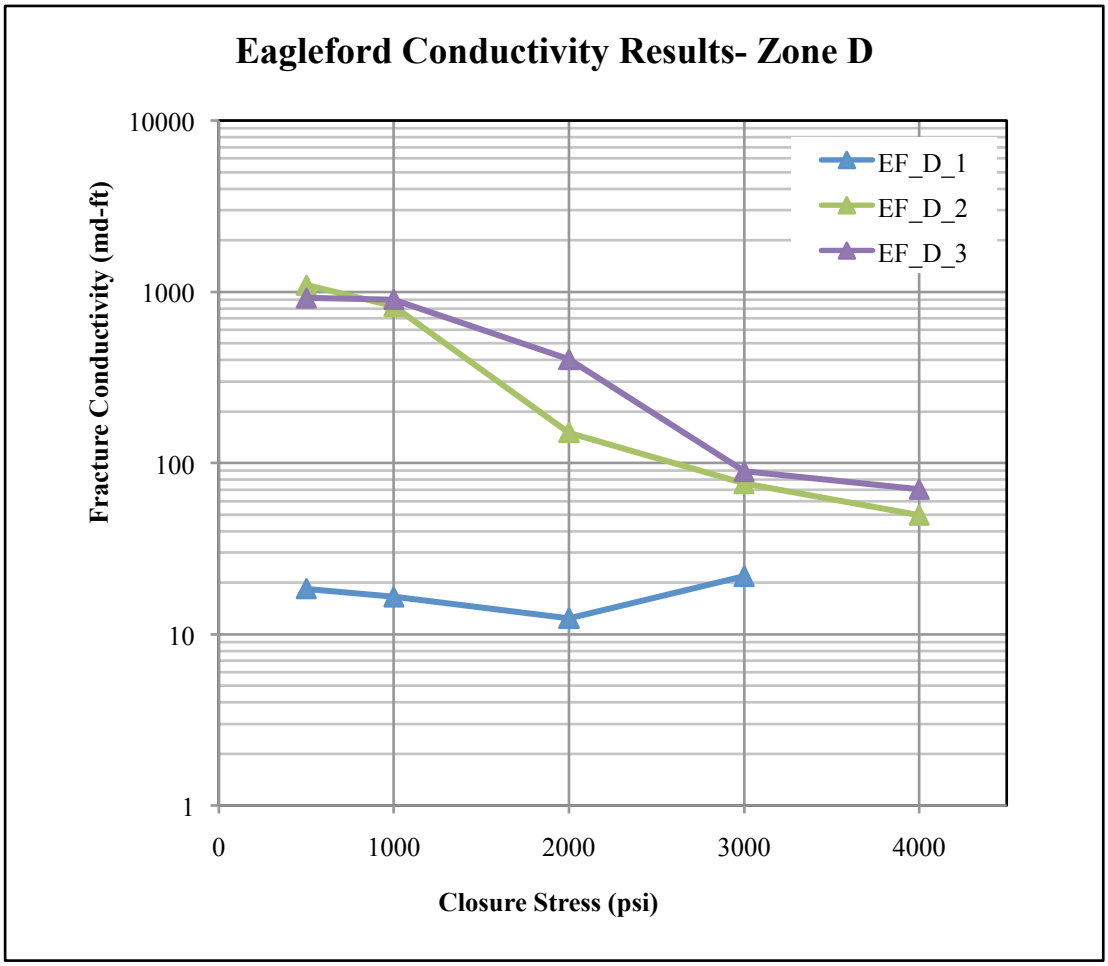

Fig. 29: Acid Fracture Conductivity for Zone D (EF_D_1 Contains Error)

3.4 Results for Test Condition #3

The total dissolved surface etching volume for the two Eagle Ford samples tested under test condition #3 with 15wt% HCl, 10 minute contact time, and ambient temperature with corresponding acid fracture conductivity values are shown in **Table 6.**

Table 6: Total Left and Right Etching Volumes (in^3)

Sample	Test Condition	Left Etching Volume (in^3)	Right Etching Volume (in^3)	Conductivity (md-ft) Resulting from Closure Stress				
				500 psi	1000 psi	2000 psi	3000 psi	4000 psi
EF_C_4	3	0.130	0.253	405	155	56	21	8
EF_D_4	3	0.129	0.667	665	625	448	181	24

3.4.1 EF_C_4

Sample EF_C_4 was tested under test condition #3: 15wt% HCl for 10 minutes and ambient temperature. The sample experienced large total surface etching volumes for both right and left cores, $0.253in^3$ and $0.130in^3$, respectively. Roughness etching patterns were present on both core sides, shown in **Fig. 30**. The darker colorations on the rock sample is from the post-water flush of the acid fracturing experiment. The surface etching volume for EF_C_4 is much larger than those for EF_C_1 through EF_C_3.

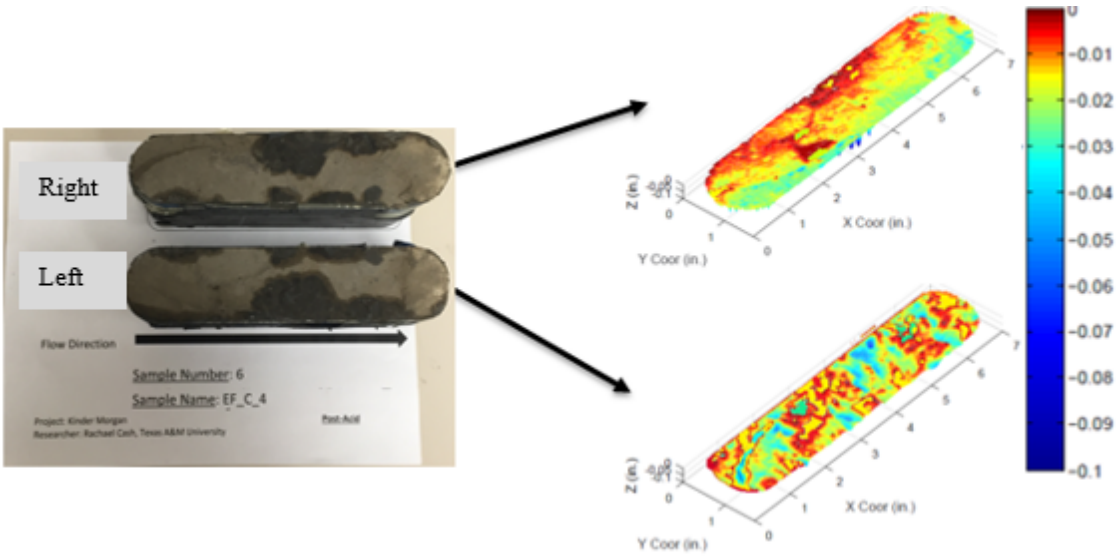

Fig. 30: Post Sample Surface Image and Difference in Surface Profile of EF_C_4. Right and Left Etching Volumes are 0.253 in^3 and 0.130 in^3 respectfully.

The higher surface etching volume compared to other zone C samples is unexpected as the acid contact time was lower and ambient temperature used. Although there were sizable etching volumes dissolved during the acid fracturing experiment, sample C_4 was unable to sustain fracture conductivity with increasing closure stress, shown in **Fig. 31**. Starting at an initial conductivity of 405mD-ft, the sample ended with a conductivity of 8mD-ft. Due to the highly variable degree of surface etching between right and left core halves, the surface asperities could not sustain a large enough area of contact to keep the fracture opened. Furthermore, the lower acid contact time of 10 minutes and 15wt% HCl had a negative impact on the fracture conductivity.

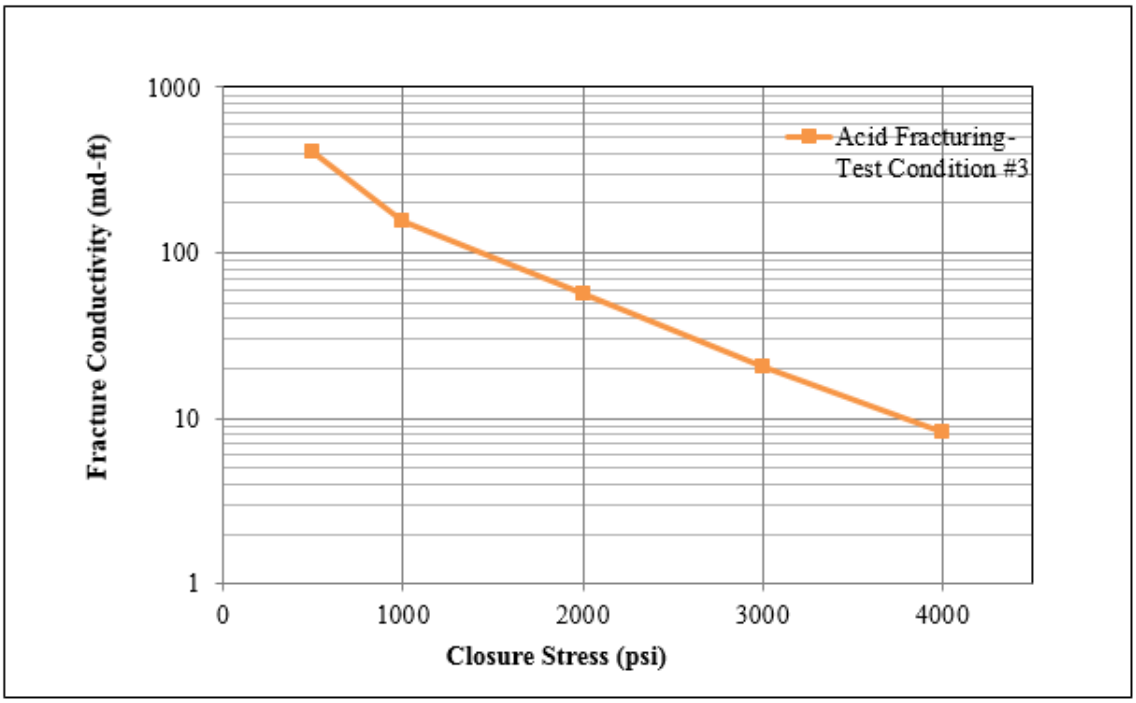

Closure Stress (psi)	k_f-w (md-ft)
500	405
1000	155
2000	56
3000	21
4000	8

Fig. 31: Acid Fracture Conductivity for EF_C_4

3.4.2 EF_D_4

EF_D_4 was also tested under test condition #3. The surface etching results are shown in **Fig. 32**. The right core had channeling etching patterns, with one large

undissolved peak region on the left side of the sample. The right core total dissolved etching volume was 0.667in^3. The left core had predominantly a channeling etching pattern, with large channel formation on the outer right side. The left total etching volume was 0.129in^3.

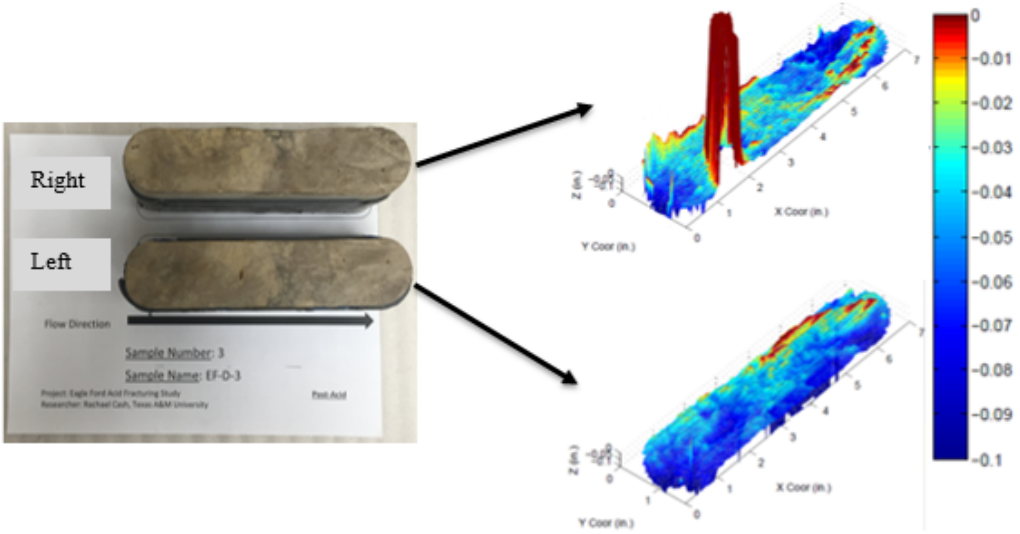

Fig. 32: Post Sample Surface Image and Difference in Surface Profile of EF_D_4. Right and Left Etching Volumes are 0.667 in^3 and 0.129 in^3, respectfully.

Fig. 33 shows that the lack of acid contact time, acid concentration strength, and ambient temperature had negative effects on the conductivity results of sample EF_D_4. Dominant channeling that encompassed the majority of the left and right cores was unable to completely support closure stress and resulted in a lower than average initial conductivity of 665 md-ft. Acting as a pillar, the undissolved peak region on the right sample surface allowed the fracture to remain open, ending with a conductivity of 24

md-ft.

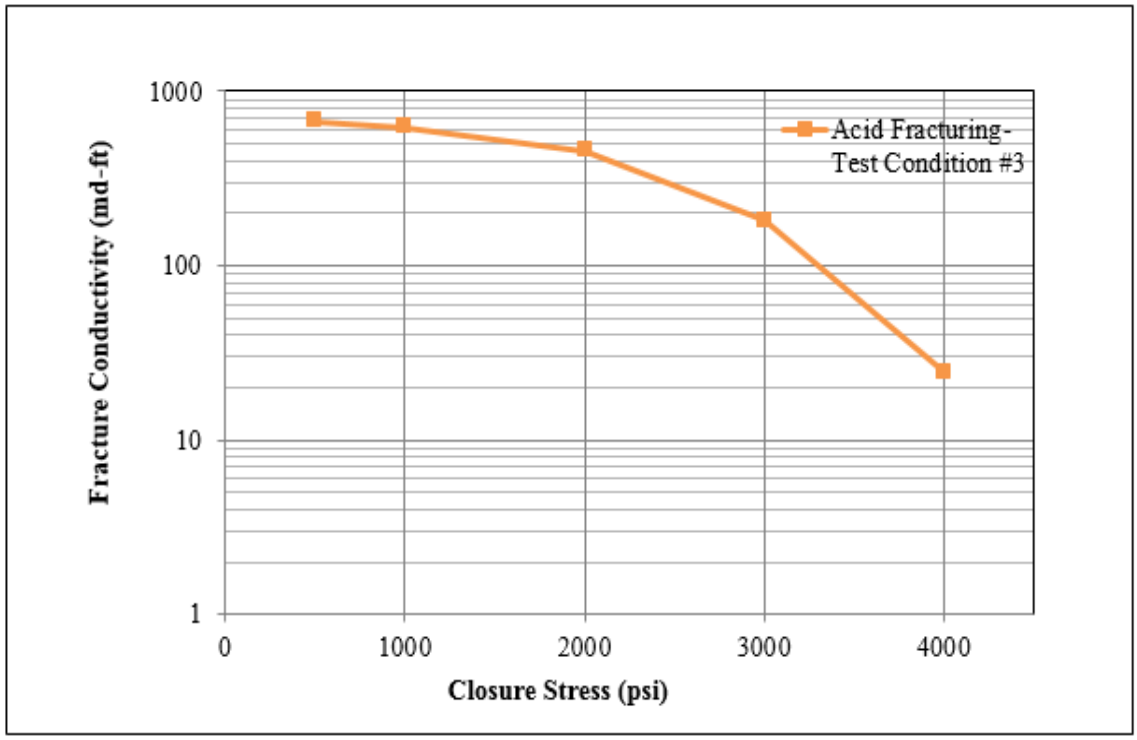

Closure Stress (psi)	k_f-w (md-ft)
500	405
1000	155
2000	56
3000	21
4000	8

Fig. 33: Acid Fracture Conductivity for EF_D_4

3.5 Parametric Study of Acid Fracturing Conductivity in the Eagle Ford Shale

The effects of etching pattern, acid concentration, carbonate content, and Brinell Hardness number on the created acid fracture conductivity are analyzed in this section.

3.5.1 Effect of Etching Pattern on Acid Fracture Conductivity

Throughout this study four distinct etching patterns were observed and are shown in **Fig. 34**: non-etching, channeling, roughness, and turbulent surface etching patterns.

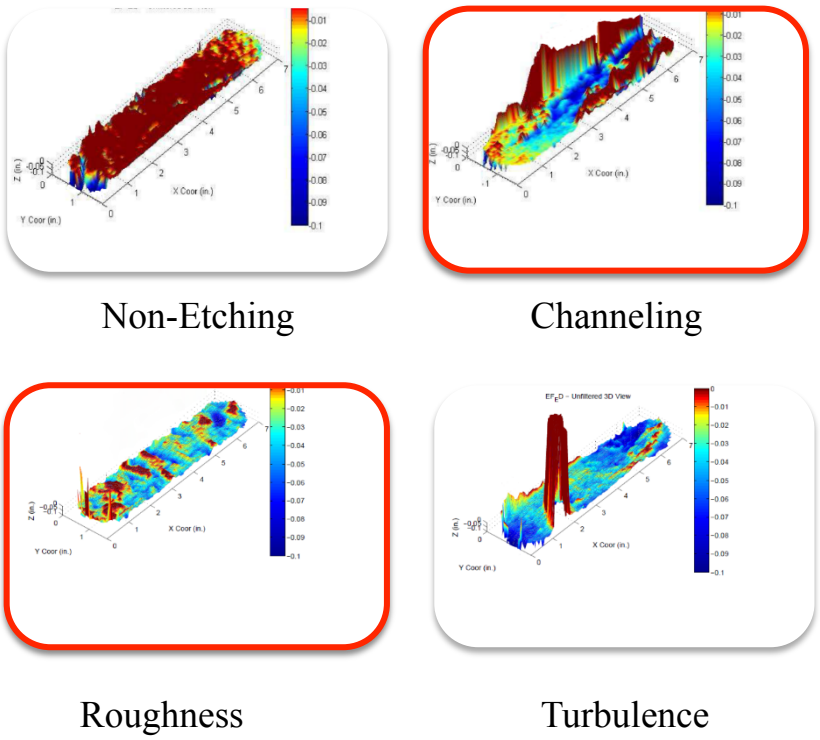

Fig. 34: Four Observed Etching Patterns (Modified from Pournik, 2009)

Of the four etching patterns, the most desirable are channeling and roughness, as sufficient surface asperities remain to keep the fracture competent under closure stress. Channeling and roughness etching patterns occur when there is a high volume of surface etching. Therefore, generally the higher the surface etching volumes, the more likely roughness and channeling surface etching patterns will be present, and thus higher sustained acid fracture conductivity, shown in **Fig. 35**.

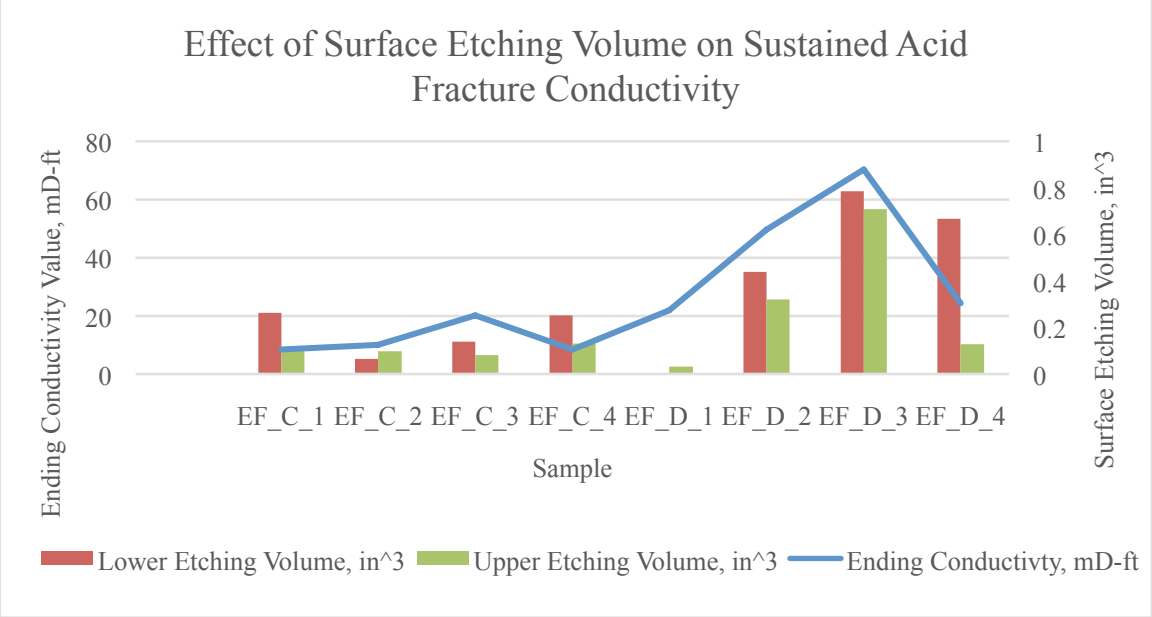

Fig. 35: Effect of Surface Etching Amount on Sustained Acid Fracture Conductivity

Shown in **Fig. 36**, in roughness etching patterns, conductivity is controlled by etching and rock strength whereas in channeling, channels control conductivity. The latter phenomena was originally observed in carbonate formations and is now also observed in the Eagle Ford shale from experimental results.

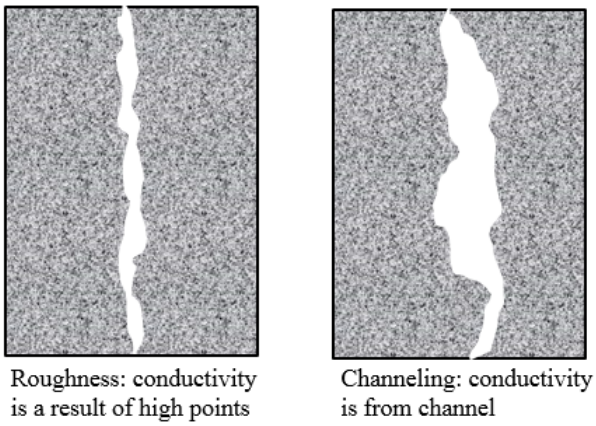

Fig. 36: Effect of Surface Structure on Conductivity. From Melendez, 2007

When roughness was observed, the higher the rock strength determined from Brinell Hardness Number, the higher the resulting conductivity. Stress is absorbed on the high points, or points of support, created from the roughness pattern which helps even out the stress distribution on the fracture. In turn, the fracture is able to support and remain opened under additional closure stress. The basic methodology of the ability of the high points to support closure stress is similar to pillar support in underground mining; the highest stress distribution is on the points of contact.

Of the samples that displayed channeling, the samples were able to remain open under closure stress and experienced very high conductivity values for the shale samples. When a channeling surface etching results, the conductivity is dependent upon the channel, specifically the height of the created channel. At higher closure stress, higher conductivity can be achieved by small, hard to deform channels that are not deformed by rock expansion or in-situ stress (Melendez et al., 2007). Smaller scale channels, i.e.

H=0.1ft., can support higher closure stresses. Described in **Fig. 37**, as the height of channels increases, the fracture is more susceptible to closure, as there are no high points or surface asperities to provide support. At the larger scale, i.e. H=100ft., the channel is most likely to close when the total fracture height is equal to the length of the fracture. The creation of a larger channel encompassing the right and left cores occurred in sample EF_D_4, where the fracture was unable to remain open.

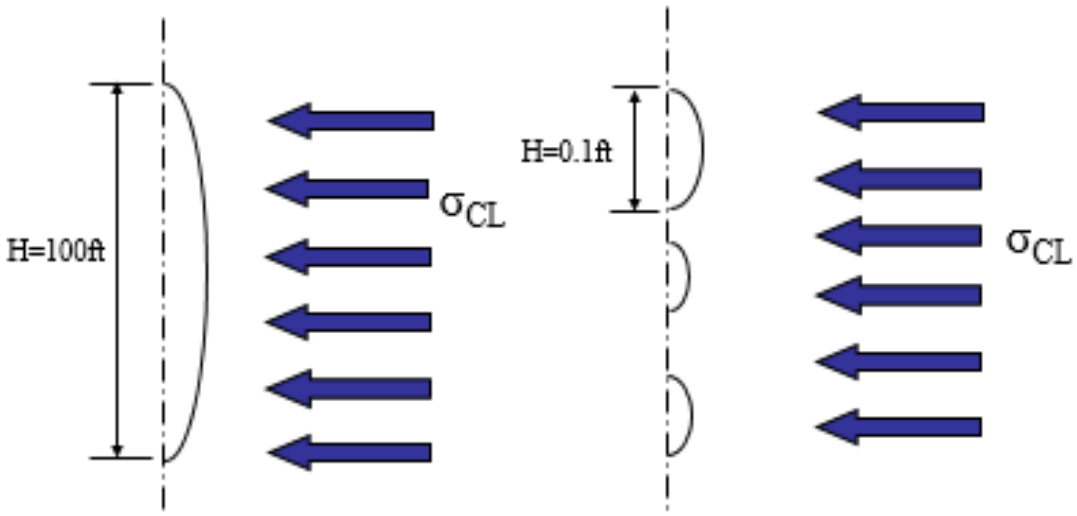

Fig. 37: Effect of Surface Structure on Conductivity. From Melendez, 2007

If there is no surface etching, there is nothing to help keep the fracture opened. Therefore, non-etching does not provide sufficient surface asperities to keep the fracture opened under additional closure stress, which was shown in sample EF_D_1, the lowest overall conductivity values in this study.

3.5.2 Effect of Acid Concentration on Acid Fracture Conductivity

Using test conditions #1 and #2, the effect of varying acid concentration on the Eagle Ford shale zones C and D was observed and the results are included in **Table 7**.

Table 7: Resulting Conductivity for Varying Acid Concentrations in Test Condition #1 and #2

Sample	Test Condition	Left Etching Volume (in^3)	Right Etching Volume (in^3)	Conductivity (md-ft) Resulting from Closure Stress				
				500 psi	1000 psi	2000 psi	3000 psi	4000 psi
EF_C_1	1	0.113	0.264	1010	976	443	132	9
EF_C_2	1	0.097	0.065	806	444	227	69	10
EF_C_3	2	0.081	0.138	491	242	45	42	20
EF_D_1	1	0.033	0.004	18	17	12	21	-
EF_D_2	1	0.320	0.440	1093	825	150	76	50
EF_D_3	2	0.710	0.785	920	901	403	89	70

For zones C and D, an acid concentration of 28wt% HCl yielded higher initial conductivity than 15wt% HCl. Sample EF_D_1 is an exception to this, as the rock was broken during the conductivity experiment and therefore should not be included in any trends. However, as shown in **Fig. 38**, higher acid concentrations did not always yield higher conductivity values as additional closure stress was applied.

For zone C, EF_C_1 and EF_C_2 started with an initial conductivity higher than that of EF_C_3. However, as the closure stress increased, EF_C_3 was able to sustain higher conductivity than either of the other C samples. The same process occurred for samples from zone D. With 15wt% HCl, samples were able to sustain fracture conductivity at higher values, compared to 28wt% HCl, due to the weakening of the rock that occurs when using 28wt% HCl. Samples EF_C_3 and EF_D_3, which had acid concentrations of 15wt% HCl, ended with conductivity values that were on average 54% higher than samples with 28wt% HCl. In the field 15wt% HCl is recommended instead of 28wt%. Even though higher initial conductivity is achieved with 28wt% HCl, fracture conductivity can be sustained at higher rates with 15wt% HCl.

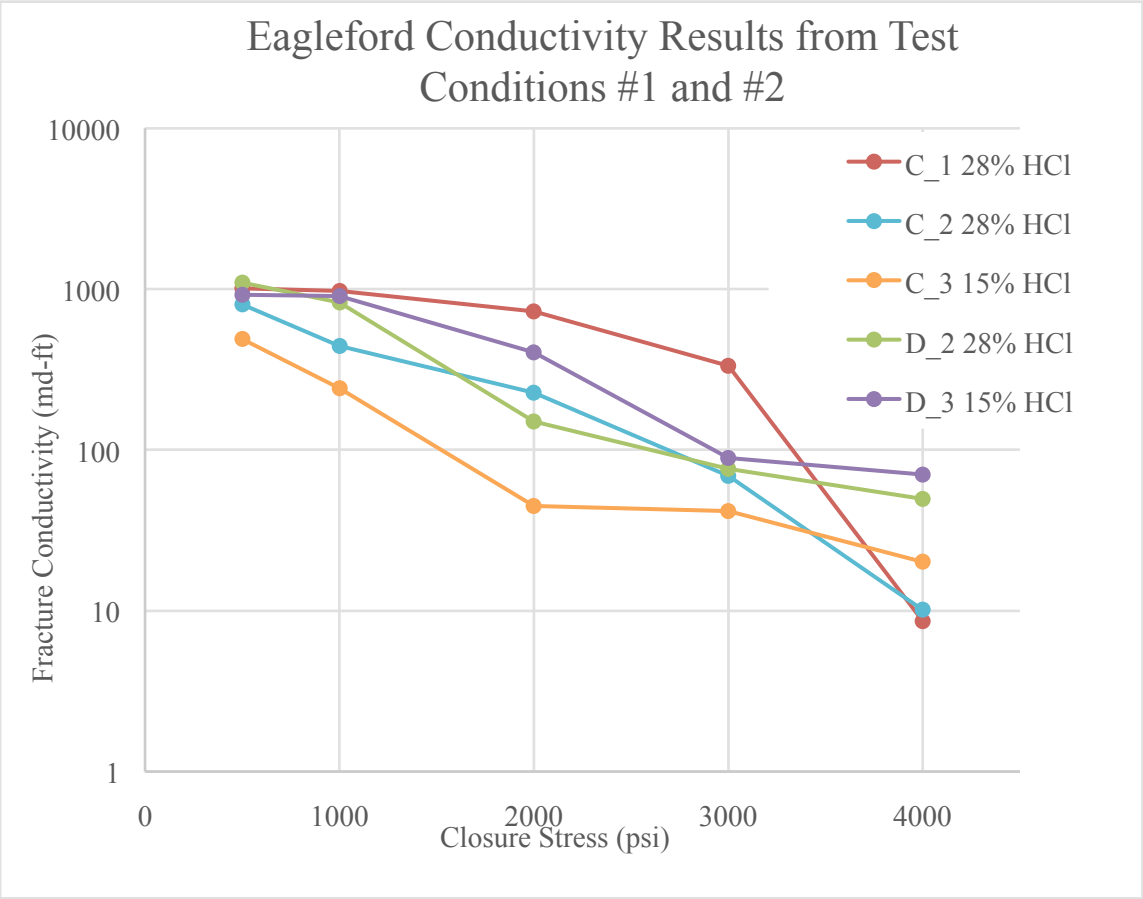

Fig. 38: Eagle Ford Test Results for Test Conditions #1 and #2 (EF_D_1 is not shown)

3.5.3 Effect of Calcite Content on Acid Etching and Acid Fracture Conductivity

An X-Ray Diffraction (XRD) analysis was performed on samples from the three zones used in this study and the results of the analysis are shown in **Fig. 39**. Since all samples from zones C and D were cut from the individual outcrop rocks, XRD analyses were completed for each zone. The XRD results for each sample were averaged for total zone C, and zone D values.

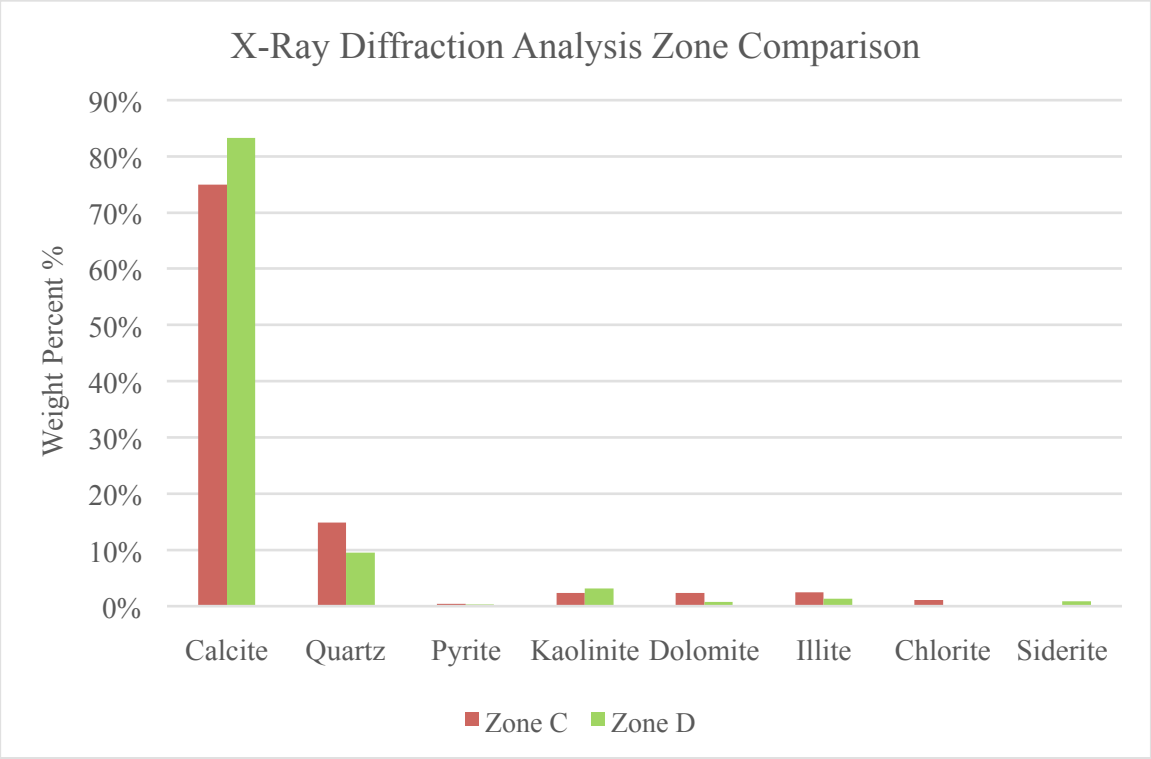

Fig. 39: X-Ray Diffraction Analysis Results for Eagle Ford Shale Zones C and D

From zone C to zone D, the calcite content of the samples increased approximately 11%. The quartz content was a small degree higher in zone C as compared to zone D. Zone D samples exhibit more characteristics of an Austin Chalk rock, therefore have on average higher calcite content and lower quartz content than lower zone Eagle Ford samples. When higher calcite content was present, channeling and surface roughness etching patterns were more prevalent, thus higher etching volumes, as shown in **Fig. 40**, and conductivity values, as shown in **Fig. 41**. On average, the higher the calcite content, the more optimistic the results expected for field tests.

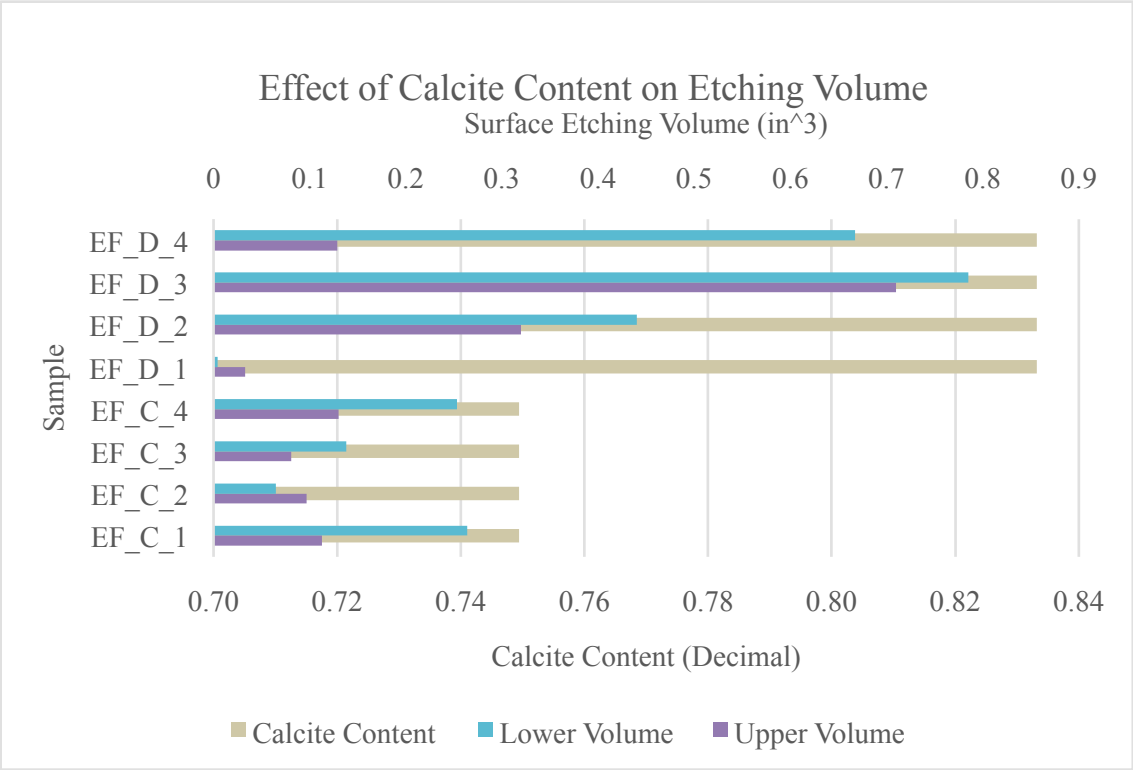

Fig. 40: Effect of Calcite Content on Surface Etching Volume

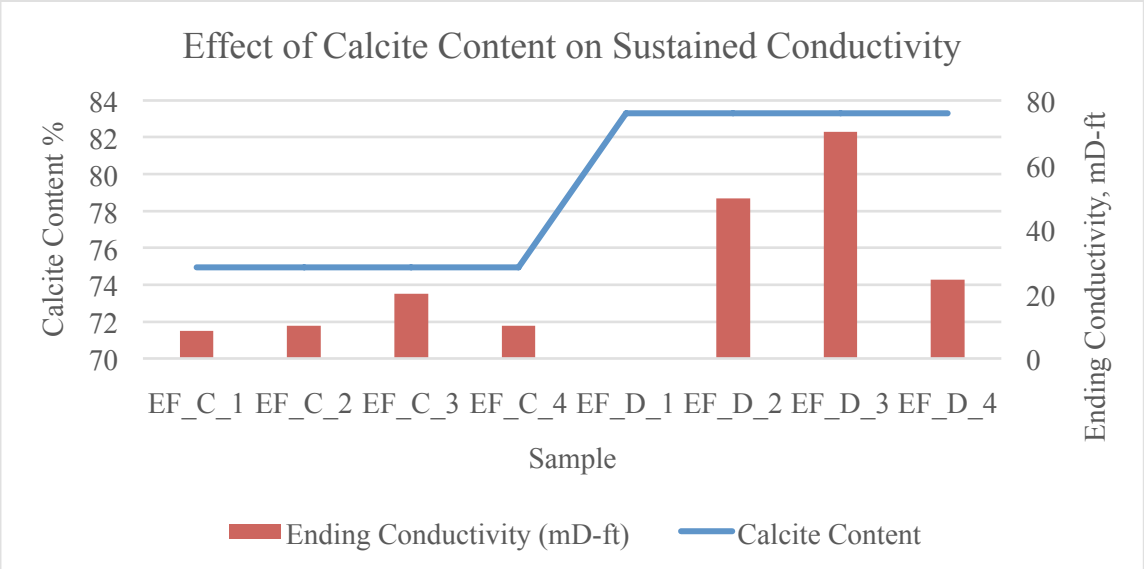

Fig. 41: Effect of Calcite Content on Sustained Conductivity

The smaller contributors to the mineral composition for zone C and D samples are shown in **Fig. 42**.

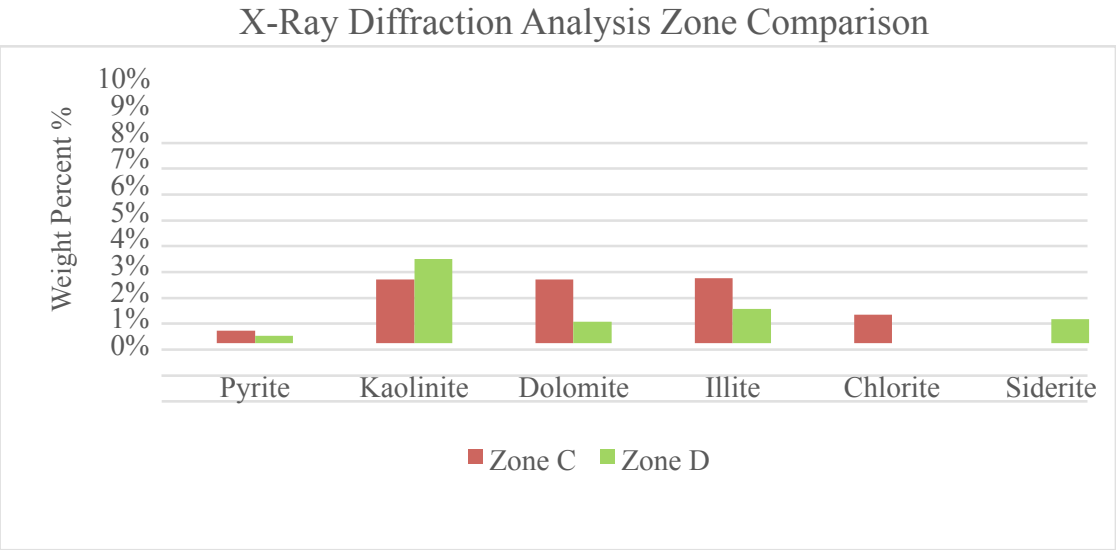

Fig. 42: X-Ray Diffraction of Zones C and D Comparison of Smaller Mineral Composition Contributions

On average, zone C samples exhibited higher clay content than zone D. This is also because zone D is compositionally more similar to the Austin Chalk than Eagle Ford shale.

3.5.4 Effect of Rock Strength Properties on Acid Fracture Conductivity

The Brinell Hardness Numbers were recorded for six Eagle Ford 1" x 1 ½" core plug samples tested pre-acid, shown in **Fig. 43**. Hardness tests were not completed for EF_C_4 and EF_D_4 as rock strength properties from the Tripathi and Pournik study

were not available for comparison. Hardness measurements record the resistance of the rock sample to penetration by a harder material under a specific load (Mueller and Amro, 2015).

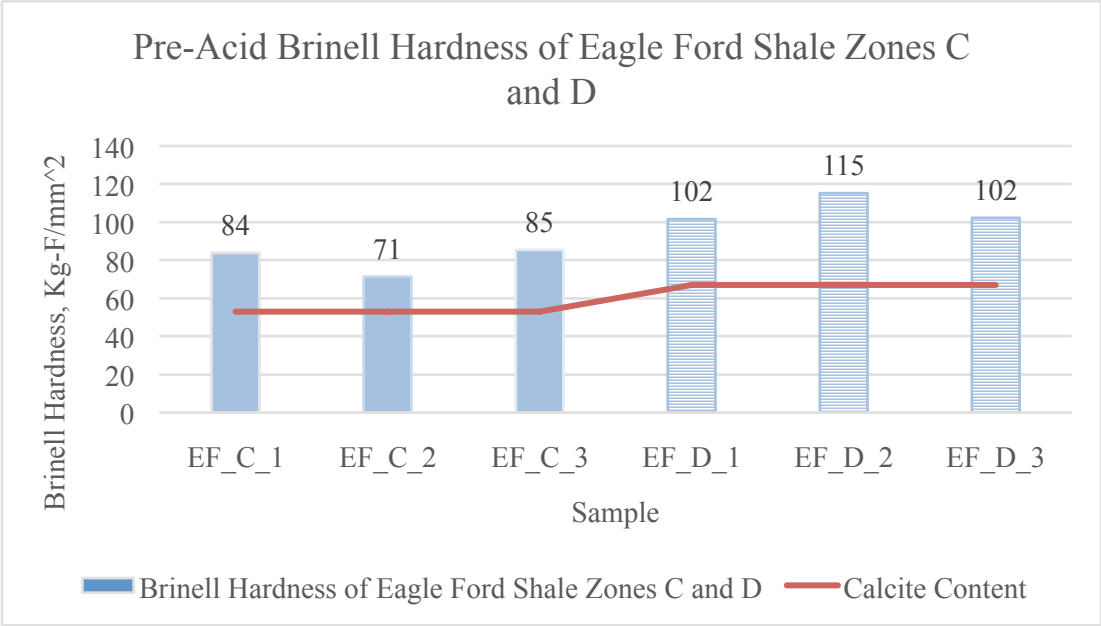

Fig. 43: Hardness Results for Eagle Ford Shale Samples

The higher hardness values occurred in samples of higher calcite content, and thus higher surface etching and resulting fracture conductivity which was the case for zone D. Zone C exhibited a weaker mineral composition with less calcite as compared to zone D, resulting in lower hardness value. Zone D exhibited a higher hardness on average, reflective of the higher content of stronger minerals such as calcite and quartz.

A direct correlation can be drawn between Brinell Hardness Number and resulting acid fracture conductivity in high carbonate containing shale formations; the

higher the hardness value, the more desirable surface etching pattern and resulting acid fracture conductivity. The higher the hardness value, the more likely the sample was to have sustained conductivity, which is shown in **Fig. 44**. Since Brinell Hardness tests were performed prior to acid, the calcite areas of the rock samples were dissolved (calcite in zone D) leaving behind stronger minerals such as quartz to act as pillars propping the fracture open. Whereas zone C initially had less calcite and more weak minerals, such as clays, undissolvable by HCl, thus lower surface etching and fracture conductivity.

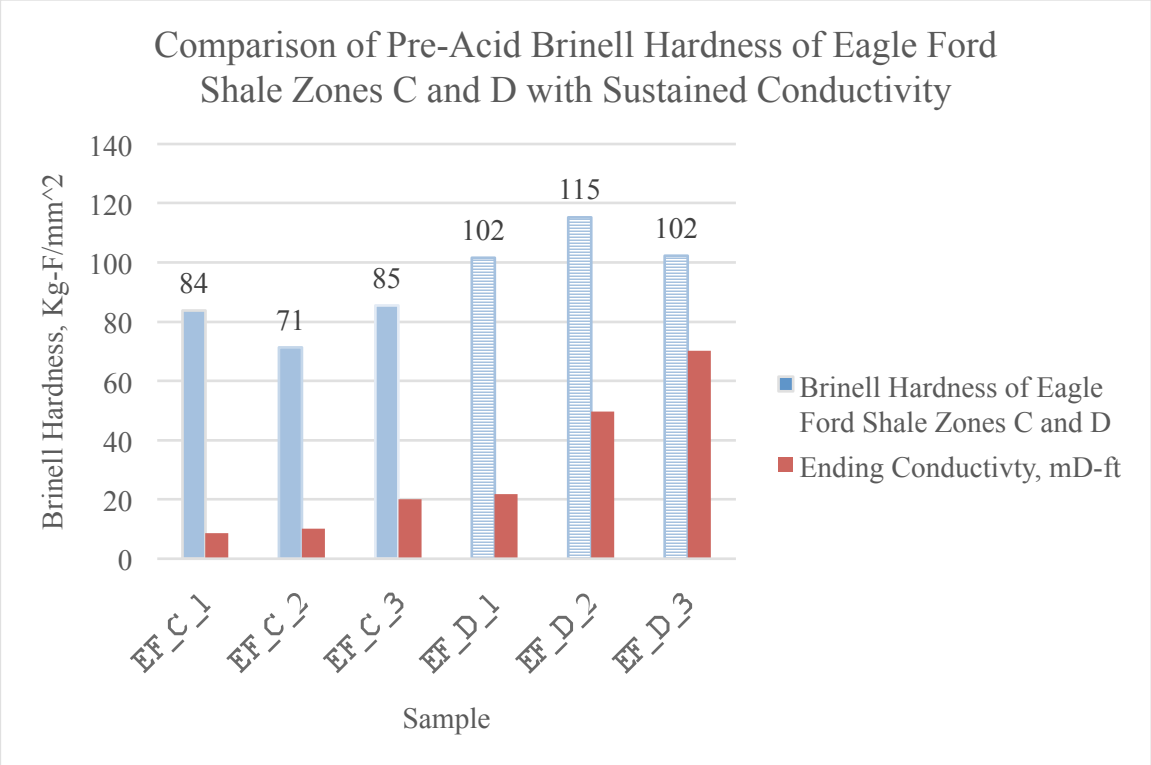

Fig. 44: Hardness and Resulting Sustained Conductivity for Eagle Ford Shale Samples

Zone C had lower hardness values and was unable to sustain fracture conductivity as the closure stress increased. The lack of differential etching resulted in fewer channeling and roughness etching patterns, which in turn lead to fracture closure. Furthermore, since zone C was composed of weaker rocks, the additional closure stress could not be sustained by the formation. Zone D, with higher hardness values, was able to sustain fracture conductivity under additional closure stress. Due to the stronger minerals and higher degree of channeling and roughness etching patterns, the fracture was able to remain opened.

3.5.5 Comparison with Tripathi and Pournik Study

Test condition #3, consisting of 15wt% HCl, 10 minute contact time, and ambient temperature was created to better mimic the Tripathi and Pournik study. The experimental conditions are listed in **Table 8**. The Tripathi and Pournik study used 15wt% HCl with an injection rate of 30mL/min and ambient temperature.

Table 8: Comparison of Experimental Conditions

Condition	Current Study	Tripathi and Pournik
Core Sample Origin	Eagle Ford outcrop (zones C and D)	Eagle Ford Outcrop
Core Sample Size and Shape	1.7" x 7" x 6" API conductivity cell shape	1.5" x 6" cylindrical shape
Calcite Content	Eagle Ford zone C average: 75% Eagle Ford zone D average: 84%	49 wt.% (FTIR)
Acidizing Conditions	Test Condition #3: • Acid: 15wt% HCl • Injection rate: 1L/min • Temperature: ambient • Contact time: 10min	Acid: 15wt% HCl Injection rate: 30mL/min Temperature: ambient Contact time: 10min

The calcite content recorded from X-Ray diffraction analysis in this study was much higher than the calcite content recorded in the Tripathi and Pournik study using Fourier transform infrared spectroscopy (FTIR). FTIR uses an infrared spectrum of absorption whereas XRD uses diffraction of crystalline structures and provides more definitive structural information (Loye, 2013).

The Tripathi and Pournik study had less optimistic results for acid fracturing the Eagle Ford shale compared with the results from this study, which are compared in **Table 9**. Tripathi and Pournik results are estimated as exact data points were not given.

Table 9: Etching and Conductivity Results for Test Condition #3

Sample	Contact Time (min)	Acid wt.%	Left Etching Volume (in^3)	Right Etching Volume (in^3)	Conductivity (md-ft) Resulting from Closure Stress				
					500 psi	1000 psi	2000 psi	3000 psi	4000 psi
EF_C_4	10	15wt%	0.130	0.253	554	345	181	30	10
EF_D_4	10	15wt%	0.129	0.667	665	625	448	181	24

The conductivity values for EF_C_4 and EF_D_4 were plotted with the results from the Tripathi and Pournik study (shown in red) in **Fig. 45**.

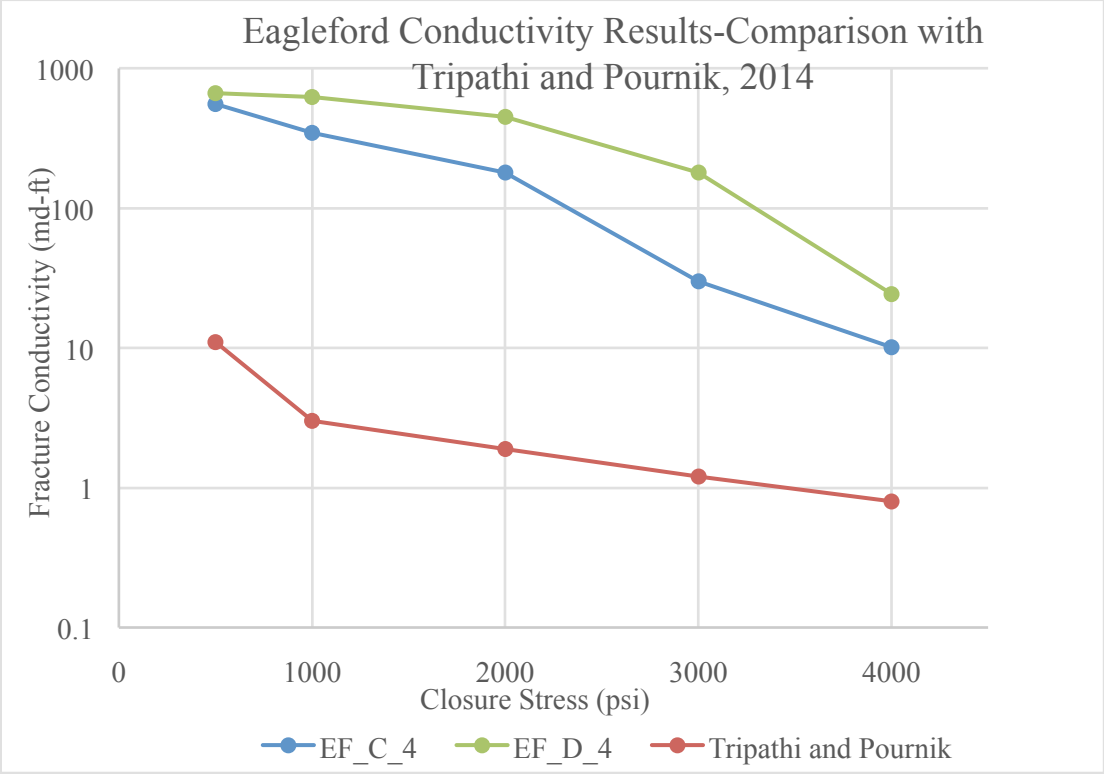

Fig. 45: Comparison of Acid Fracture Conductivity Results with Tripathi and Pournik Study (2014)

The difference in conductivity values results from their use of a lower injection rate, varying sample composition, and sample size. One major difference results from differences in sample composition due to the high heterogeneity of the Eagle Ford shale. On average, the samples used in this study had a higher calcite content, thus higher potential for dissolving capacity during acid fracturing. Another major difference in the outcome of results is due to the difference in sample size. Due to lab limitations, the exact setup of the Tripathi and Pournik study could not be recreated.

CHAPTER IV
CONCLUSION AND FUTURE WORK

4.1 Conclusion and Future Work

From the experimental results and analysis, the following conclusions can be made for acid fracturing high carbonate containing shale formations, namely the Eagle Ford shale:

I. Etching pattern: Channeling and roughness are the most desired etching pattern as they allows for sufficient surface asperities to keep fractures opened under closure stress
II. Acid Concentration: 15wt% HCl is recommended. Even though higher initial conductivity is achieved with 28wt% HCl, fracture conductivity can be sustained at higher rates with 15wt% HCl.
III. Calcite content of shale samples: The higher the initial calcite content of shale samples, the highly likelihood of channeling and roughness etching patterns and thus higher resulting fracture conductivity.
IV. Rock strength properties: The higher the Brinell hardness number, the higher both the initial fracture conductivity and sustained conductivity values.

Overall, there are optimistic results for acid fracturing the Eagle Ford shale in areas of high calcite content with high Brinell Hardness Number, where created fractures

are more likely to experience channeling and roughness etching patterns which in turn result in both higher and more sustained conductivity values.

Future work is to obtain both outcrop and core samples from Eagle Ford zone B to further test the effects of acid fracturing in the production zone. Cores would provide a more realistic representation to field conditions compared to outcrop rocks, as outcrop rocks are exposed to weathering and are not fully representative of in-situ conditions. Further studies also can study the effects of the use of proppant in addition to acid fracturing. The combination of proppant used in conjunction with acid would allow the microfractures to be reached with the acid while maintaining competent larger fractures with the proppant. If additional Eagle Ford samples are available, future testing could also be completed to determine the effect of bedding orientation, parallel or perpendicular, on acid fracturing and resulting conductivity.

REFERENCES

Abass, H.H., Al-Mulhem, A.A., Alqam, M.S., et al. 2006. Acid Fracturing or Proppant Fracturing in Carbonate Formation? A Rock Mechanic's View. Presented at the SPE Annual Technical Conference and Exhibition, San Antonio, Texas, 24-27 September. SPE 102590-MS. http://dx.doi.org/10.2118/102590-MS.

Antelo, L. F., Zhu, D., & Hill, A. D. 2009. Surface Characterization and its Effect on Fracture Conductivity in Acid Fracturing. Presented at the SPE Hydraulic Fracturing Technology Conference, The Woodlands, Texas, 19-21 January. doi:10.2118/119743-MS.

Ashby, M.F., Shercliff, H., and Cebon, D. "Materials: Engineering, Science, Processing and Design," Elsevier, Amsterdam, 2013, p. 167.

Deng, J., Hill, A.D., and Zhu, D. 2011. A Theoretical Study of Acid-Fracture Conductivity under Closure Stress. *SPE Prod. & Oper.* 26(1): 9-17. Society of Petroleum Engineers. doi:10.2118/124755-PA

Donovan, A. D., and S. Staerker, 2010. Sequence stratigraphy of the Eagle Ford (Boquillas) formation in the subsurface of South Texas and the outcrops of West Texas: Gulf Coast Association of Geologic Societies Transactions, v. 60, p. 861–899.

Donovan, A.D., S. Staerker, A. Pramudito, et al. 2012,. The Eagle Ford Outcrops of West Texas: A Laboratory for Understanding Heterogeneities within Unconventional Mudstone Reservoirs. *GCAGS Journal*. V.1: 162-185

Dunham, R. J., 1962, Classification of carbonate rocks according to depositional texture. In: Ham, W. E. (ed.), Classification of Carbonate Rocks: American Association of Petroleum Geologists Memoir, p. 108-121.

Economides, M.J., and Nolte, K.G.: "Reservoir Stimulation," Schlumberger, Prentice Hall, Englewood Cliffs, 2nd Ed., 1989.

Economides, M.J., Hill, A.D., Ehlig-Economidies, et al. *Petroleum Production Systems,* second edition. Westford, Massachusetts: Prentice Hall, 2nd Ed., 2012.

Gardner, R.D., Pope, M.C., Wehner, M.P., et al. 2013. Comparative Stratigraphy of the Eagle Ford Group Strata in Lozier Canyon and Antonio Creek, Terrell County, Texas. *GCAGS Journal*. V.2: 42-52.

GeoScienceWorld: American Mineralogist. 2014. Dolomite Packing Structure. http://ammin.geoscienceworld.org

Gehring, A. 2016. The Effect of Rock Properties on Fracture Conductivity in the Eagle Ford. Master's thesis, Texas A & M University.

Gibson, A.T. 2014. Paleo environmental Analysis and Reservoir Characterization of the Late Cretaceous Eagle Ford Formation in Frio County, Texas, USA. A Master's thesis, Golden, Colorado: Colorado School of Mines. http://dspace.library.colostate.edu/webclient/DeliveryManager/digitool_items/csm01_storage/2014/04/21/file_1/281061

Goodman, R.E.: "Introduction to Rock Mechanics," Jones Wiley & Sons, New York, 1980, p.199.

Gomaa, A. M., & Nasr-El-Din, H. A. 2009. Acid Fracturing: The Effect of Formation Strength on Fracture Conductivity. Presented at the SPE Hydraulic Fracturing Technology Conference, The Woodlands, Texas, 19-21 January. SPE-119623-MS.doi:10.2118/119623-MS

Joel, E. O., & Pournik, M. 2011. Does Rock Really Weaken During Acid Fracturing Operations? Presented at the SPE Production and Operations Symposium, Oklahoma City, Oklahoma, 27-29 March. SPE-142389-MS. doi:10.2118/142389-MS

Loye, H.Z. 2013. X-Ray Diffraction: How it works and what it cannot tell us. University of South Carolina Department of Chemistry. http://www.chem.sc.edu/faculty/zurloye/xrdtutorial_2013.pdf

Lund, K., Fogler, H. S., McCune, C. C., Ault, J. W. 1976.Acidization--IV : Experimental correlations and techniques for the acidization of sandstone cores. Chemical Engineering Science 31(5): 373-380. http://hdl.handle.net/2027.42/21906>Tripathi and Pournik (2014)

Magalhaes, A.S.G, Almeida Neto, M.P., Bezerra, M. N., and Feitosa, J.P.A. 2013. Superabsorbent Hydrogel Composite with Minerals Aimed at Water Sustainability. Journal of the Brazilian Chemical Society. Vol. 24, no. 2.

Malagon, C. 2007. 3D characterization of acidized fracture surfaces. Master's thesis, College Station: Texas A&M University. http://hdl.handle.net/1969.1/5771

Malagon, C., Pournik, M., and Hill, A.D. 2008. The texture of acidized fracture surfaces: Implications for acid fracture conductivity. *SPE Prod. & Oper.* 23(3): 343-352.

McGinley, M. J. 2015. The Effects of Fracture Orientation and Anisotropy on Hydraulic Fracture Conductivity in the Marcellus Shale. Master's thesis, Texas A & M University. Available electronically from http : / /hdl .handle .net /1969 .1 /155300.

Melendez, M., Pournik, M., Zhu, D., and Hill, A.D. 2007. The Effects of Acid Contact Time and the Resulting Weakening of Rock Surfaces on Acid-Fracture Conductivity. Presented at the SPE European Formation Damage Meeting, 30 May – 1 June. SPE-107772-MS. doi:10.2118/107772-MS

Melendez, M.G. 2007. The Effects of Acid Contact Time and Rock Surfaces on Acid Fracture Conductivity. Masters of Science, Texas A&M University. http://hdl.handle.net/1969.1/ETD-TAMU-1956.

Mou, J., Zhu, D., and Hill, A.D. 2011. New Correlations of Acid-Fracture Conductivity at Low Closure Stress Based on the Spatial Distributions of Formation Properties. *SPE Prod. & Oper.* 26(2): 195-202.

Mueller, M. & Amro, M. 2015. Indentation Hardness for Improved Proppant Embedment Prediction in Shale Formations. Presented at the SPE European Formation Damage Conference and Exhibition, Budapest, Hungary, 3-5 June 2015. SPE-174227-MS. doi: 10.2118/174227-MS

Nasr-El-Din, H. A., Al-Driweesh, S. M., Chesson, J. B., & Metcalf, A. S. 2006. Fracture Acidizing: What Role Does Formation Softening Play in Production Response? Society of Petroleum Engineers. doi:10.2118/103344-MS

Newman, M. S., Pavloudis, M., & Rahman, M. M. 2009. Importance of Fracture Geometry and Conductivity in Improving Efficiency of Acid Fracturing in Carbonates.

Presented at the Canadian International Petroleum Conference (CIPC), Calgary, Alberta, Canada, 16-18 June. PETSOC-2009-146. doi:10.2118/2009-146

Nierode, D.E. and Kruk, K.F. 1973. An Evaluation of Acid Fluid Loss Additives Retarded Acids, and Acidized Fracture Conductivity. Presented at the Fall Meeting of the Society of Petroleum Engineers of AIME, Las Vegas, Nevada, 30 September-3 October. SPE-4549-MS. http://dx.doi.org/10.2118/4549-MS.

PhotoMetrics, Inc. 2016. Field Emission Scanning Electron Microscopy (FESEM). http://photometrics.net/field-emission-scanning-electron-microscopy-fesem/

Pournik, M. 2008. Laboratory-scale fracture conductivity created by acid etching. Ph.D. dissertation, College Station: Texas A&M University.

Pournik, M., Gomaa, A. M., & Nasr-El-Din, H. A. 2010. Influence of Acid-Fracture Fluid Properties on Acid-Etched Surfaces and Resulting Fracture Conductivity. Presented at the SPE International Symposium and Exhibition on Formation Damage Control, Lafayette, Louisiana, 10-12 February. SPE-128070-MS.doi:10.2118/128070-MS

Pournik, M., Zhu, D., & Hill, A. D. 2009. Acid-Fracture Conductivity Correlation Development Based on Acid-Etched Fracture Characterization. Society of Petroleum Engineers. doi:10.2118/122333-MS

Ruffet, C., Fery, J. J., & Onaisi, A. 1998. Acid Fracturing Treatment: a Surface Topography Analysis of Acid Etched Fractures to Determine Residual Conductivity. Society of Petroleum Engineers. doi:10.2118/38175-PA

Suleimenova, A. 2015. Acid Fracturing Feasibility Study for Heterogeneous Carbonate Formation. Master's thesis, Texas A & M University. Available electronically from http : / /hdl .handle .net /1969 .1/155028.

Tripathi, D. and Pournik, M. 2014. Effect of Acid on Productivity of Fractured Shale Reservoirs. Presented at the Unconventional Resources Technology Conference, Denver, Colorado, 25-27 August. SPE-2014-1922960-MS. doi:10.15530/urtec-2014-1922960.

U.S. Energy Information Administration. 2014. Shale in the United States (4 September 2014 revision), http://www.eia.gov/energy_in_brief/article/shale_in_the_united_states.cfm

Wu, W., & Sharma, M. M. 2015. Acid Fracturing Shales: Effect of Dilute Acid on Properties and Pore Structure of Shale. Presented at the SPE Hydraulic Fracturing Technology Conference, The Woodlands, Texas, 3-5 February. SPE-173390-MS. doi:10.2118/173390-MS.

APPENDIX A

i. Eagle Ford X-Ray Diffraction Results: Zone D Sample 1

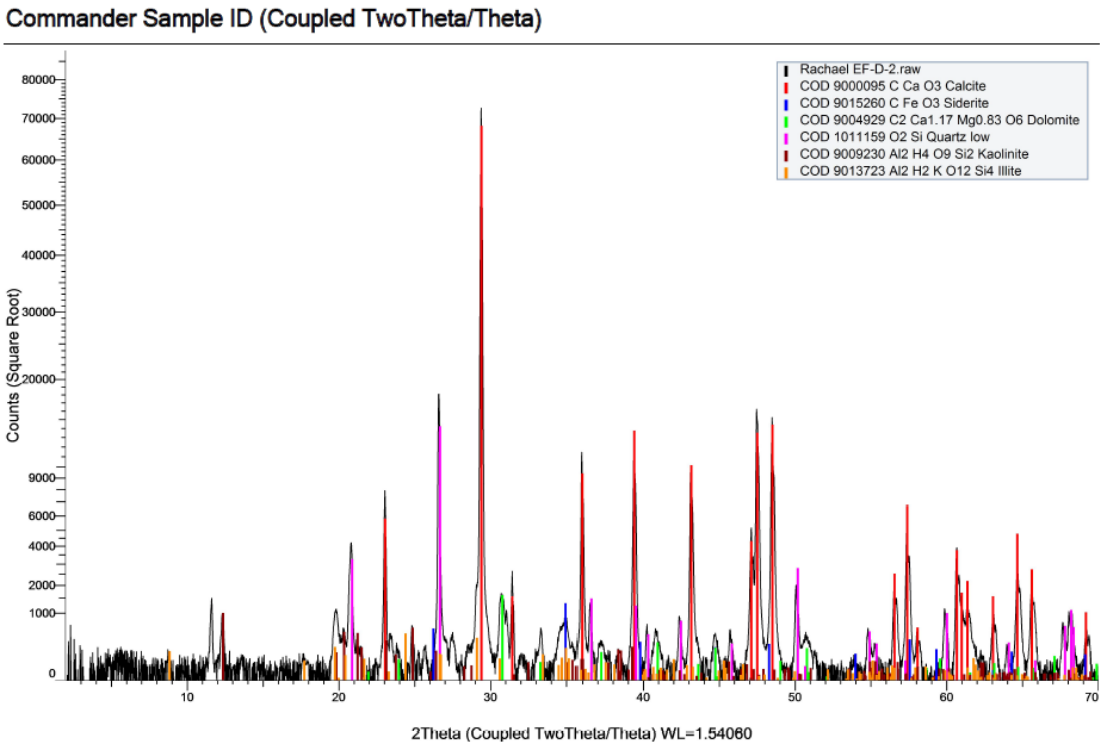

ii. Eagle Ford X-Ray Diffraction Results: Zone D Sample 2

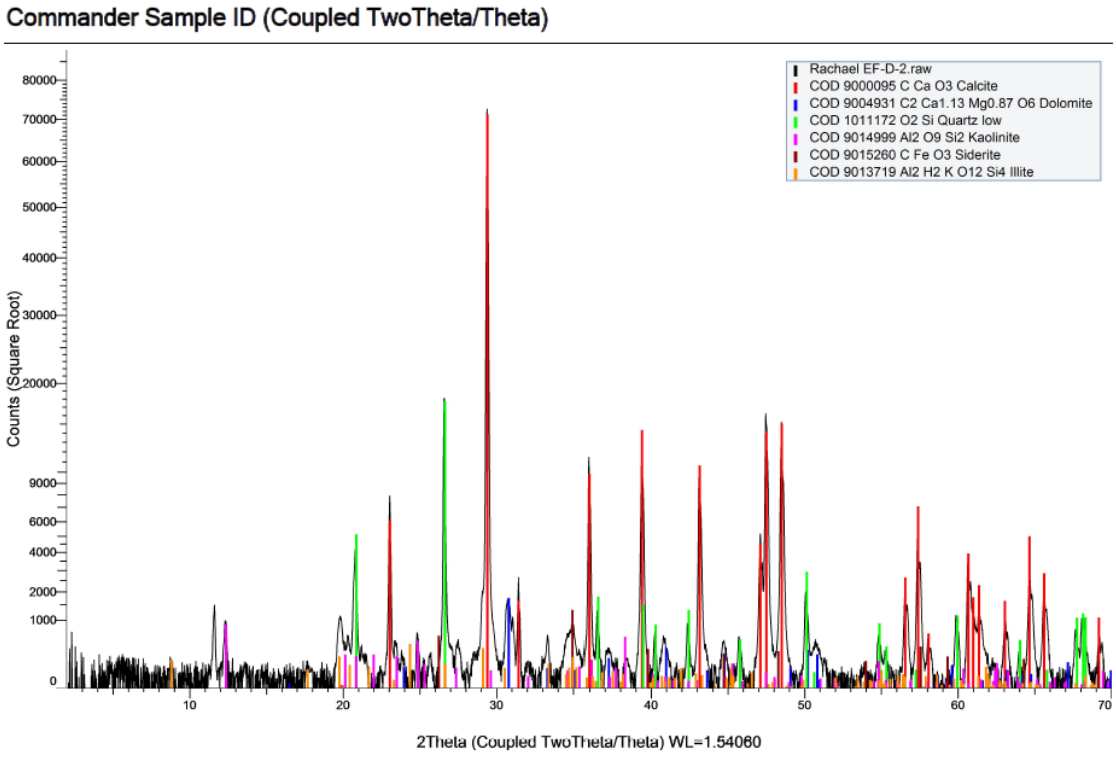

iii. Eagle Ford X-Ray Diffraction Results: Zone C Sample 1

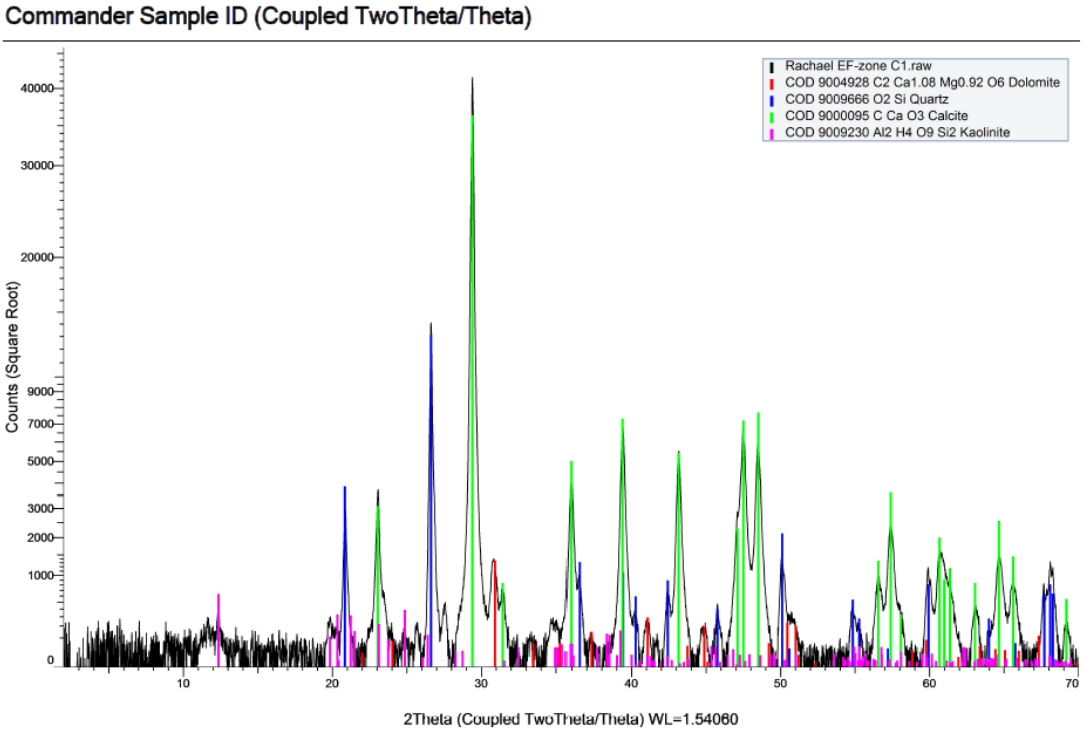

iv. Eagle Ford X-Ray Diffraction Results: Zone C Sample 2